ISSN 1028-8546

Volume XIX, Number 4
Section: En
October, 2013

Azerbaijan Journal of Physics

Fizika

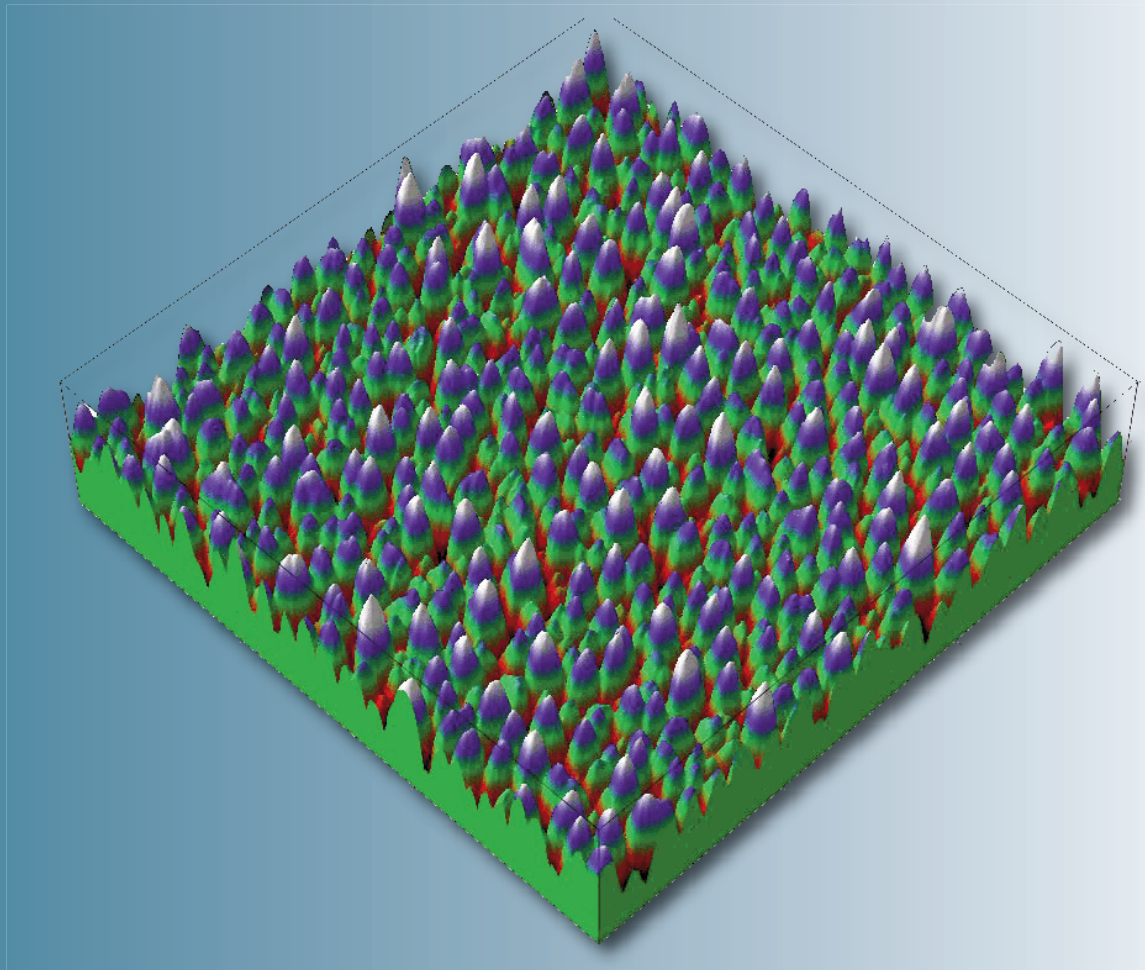

www.physics.gov.az

G.M. Abdullayev Institute of Physics
Azerbaijan National Academy of Sciences
Department of Physical, Mathematical and Technical Sciences

Published from 1995
Ministry of Press and Information
of Azerbaijan Republic,
Registration number 402, 16.04.1997

ISSN 1028-8546
vol. XVI, Number 4, 2013
Series: En

Azerbaijan Journal of Physics

FIZIKA

G.M.Abdullayev Institute of Physics
Azerbaijan National Academy of Sciences
Department of Physical, Mathematical and Technical Sciences

PUBLISHING OFFICE

33 H.Javid ave, AZ-1143, Baku
ANAS, G.M.Abdullayev Institute of Physics

Tel.: (99412) 439-51-63, 439-32-23
Fax: (99412) 447-04-56
E-mail: jophphysics@gmail.com
Internet: www.physics.gov.az

It is authorized for printing:

Published at "**SƏRQ-QƏRB**"
17 Ashug Alessger str., Baku
Typographer : Aziz Gulaliyev

Sent for printing on: __.__. 201_
Printing approved on: __.__. 201_
Physical binding:_____
Number of copies:_____200
Order:_____

INITIATION AND GROWTH CRAZES IN POLYMER COMPOSITES

T.G. MAMEDOV, M.A. KURBANOV, A.A. BAYRAMOV,
F.F. YAHYAYEV, A.F. NURALIYEV
Institute of Physics Azerbaijan National Academy of Sciences
AZ-1143, H. Javid ave., 33, Baku

A literature review of craze initiation and growth of crazes in polymer materials including composite one are presented in paper. There is a discussion concerning of mechanical properties of crazed material in paper. There is a proposed idea about new method of initialization crazy centers by the use of electric discharge plasma.

Keywords: polymer, crazes, composites, initiation, growth, electric-discharge plasma.
PACS: 77.84.Lf

1. BACKGROUND

Crazes, which are crack-like defects in polymers approximately 0,5 μm wide consisting of a web of highly strained micro fibrils, have been a subject of investigation for the past 30 years [1]. One reason for such widespread interest is the fact that these defects are likely sites for crack initiation and often cause brittle failure of an otherwise ductile polymer. Crazing is even more prominent as polymers find their way into applications where they are replacing metals. Many of these new service environments contain craze accelerating agents such as solvents, high stresses, high temperatures, and high humidities [2].

In [3] tensile drawing of the films based on high-density polyethylene in the presence of physically active liquid environments via the mechanism of delocalized solvent crazing is shown to be accompanied by the development of an open-porous structure in the polymer. Depending on the tensile strain, volume porosity of the samples can achieve up to ~ 55 vol. %, and the parameters of the porous structure (diameters of pores) lie within the nanoscale interval.

The formed nanoporous structure in the solvent-crazed samples is characterized by a highly developed surface and appears to be thermodynamically unstable; as a result, the concomitant relaxation processes lead to a partial or complete disappearance of porosity.

The effective approach providing stabilization and long-term service life of the solvent-crazed samples based on high-density polyethylene is proposed, and this approach involves a maximally complete removal of solvent from the volume of the polymer samples and their subsequent annealing.

This approach makes it possible to prepare the open-porous materials based on polyolefines with stable characteristics, and these materials present an evident practical interest.

In [4] the effect of preliminary orientation of an amorphous glassy PET via its uniaxial tensile drawing above the glass transition temperature on the deformation behavior during subsequent tensile drawing in the presence of adsorptionally active environments has been studied.

The tensile drawing of the reoriented PET samples with a low degree of preliminary orientation (below 100%) in the presence of liquid environments proceeds via the mechanism of solvent crazing; however, when a certain critical tensile strain is achieved (150% for PET), the ability of oriented samples to experience crazing appears to be totally suppressed. When the tensile drawing of reoriented samples is performed at a constant strain rate, the craze density in the sample increases with increasing the degree of preliminary orientation; however when the test samples are stretched under creep conditions, the craze density markedly decreases.

This behavior can be explained by a partial healing and smoothening of surface defects during preliminary orientation and by the effect of entanglement network. The preliminary orientation of polymers provides an efficient means for control over the craze density and the volume fraction of fibrillar polymer material in crazes.

Crazing is a form of localized plastic deformation [5]. Crazes are often mistaken for cracks because of their similarities: they form perpendicular to the principal stress direction, they act as mirrors by reflecting light off of their surfaces, and they fracture if a high enough stress is applied.

The major differences between a craze and a crack are as follows: the craze face is covered by a web of micro fibrils which bridge the craze surfaces and enable the craze to carry some load, and intersecting crazes continue to grow, independent of one another instead of joining together [6]. Crazing has been described in literature as a "tortured plastic How with a large number of voids" [6], "plastic deformation without significant lateral contraction" [6], "highly non-uniform deformation zones" [7], and "unstable local plastic deformation accompanied by volume expansion" [5].

To visually show crazing, the image was taken from the literature [8] (Fig. 1): image is a transmission electron micrograph of a polystyrene (PS) craze with clearly defined microfibrils spanning the two craze surfaces [8].

It has already been stated that crazing is an important process to consider in designing and using a frameless aircraft transparency, especially in a military application where the extreme environments and loading requirements can produce very high stresses.

The goals of this dissertation are to (a) characterize the craze growth behavior of polycarbonate as a function of stress level, (b) model the residual mechanical properties of polycarbonate at various craze levels and strain rates, and (c) determine if the total surface area of crazing is the sole factor in residual properties, or if the crazing stress plays a role.

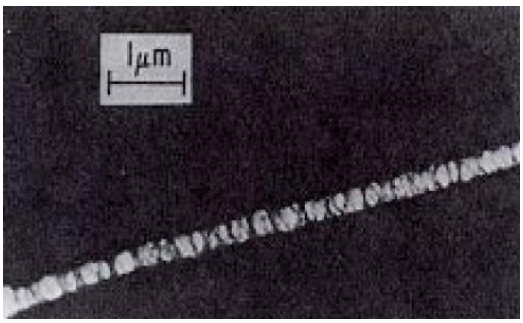

Fig. 1. Micrograph of single polystyrene craze with clearly defined fibrils [8]

The main steps to attain these goals are to:

1. Develop and validate a technique to measure the craze density of transparent polymers,
2. Characterize the craze growth behavior of polycarbonate at various crazing stresses,
3. Develop a quantitative model of the residual mechanical properties of crazed polycarbonate in terms of crazing amount, crazing stress, and strain rate, and
4. Correlate the results to craze microstructure.

Many aspects of polymer crazing are presented in the literature. They are illustrated in fig. 2 as cavitations, craze initiation, single-isolated craze growth, and bulk craze density growth.

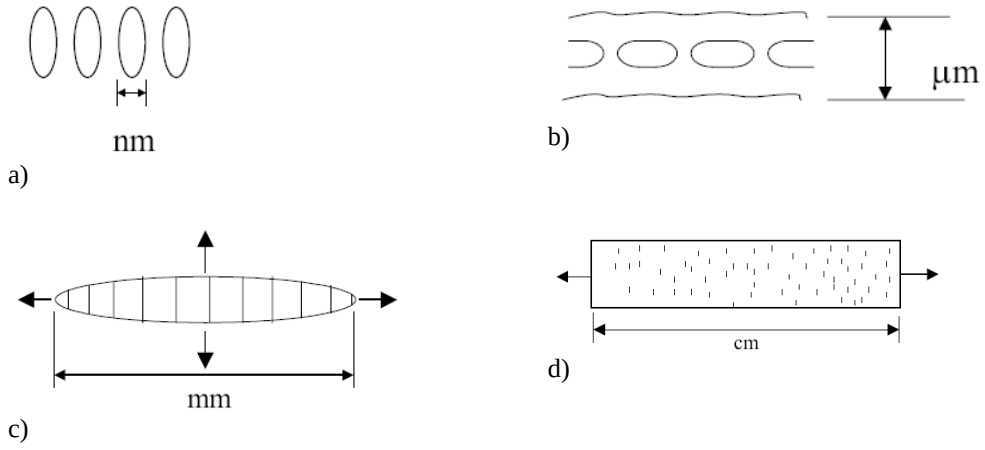

Fig. 2.

The majority of the literature discusses single craze initiation and growth, as illustrated in (b) and (c). This dissertation concentrates on the effect of bulk craze density on the mechanical properties of polycarbonate, as illustrated in (d). The bulk craze density growth rate exponentially increased as a function of stress, while the time to reach stable craze initiation decreased exponentially with increasing stress. Increasing the bulk craze density affected the properties related to fracture much more than the elastic or yield properties. For example, the yield stress and elastic modulus were insensitive to the presence of crazing while the failure strength and ductility decreased significantly with increased crazing.

2. CRAZE INITIATION

Many papers have been published in an attempt to explain the initiation of crazes [9,10], but there is still no universally accepted model for this mechanism. One difficulty in gaining insight to the initiation process is the size scale of crazes. It is believed that the first step is one of main chain motion and the formation of nano voids that are precursors to crazes. These voids are of the order of 30 nm and often form at stress concentrations like surface flaws or contaminant particles, although this is not always the case [9]. The process of these voids developing into the planar bands called crazes is not well understood. It has been postulated that the stress distribution in the region of one void causes the formation of more voids nearby, perpendicular to the maximum principal stress direction [10].

In [11] the results on biaxial critical stresses for craze initiation on the surface of cylindrical specimen of glassy polymers have been examined. A new interpretation is presented for the trend of crazing stress near pure shear state in the second quadrant of principal stress space which was observed in air at elevated temperatures. That is, an increase in the tensile stress for crazing with an increase in the magnitude of the compressive stress is interpreted not to be followed by a decrease in the dilatational stress but by development of shear yielding. On the basis of this interpretation, a new empirical criterion for craze initiation is proposed by considering the stress concentration due to surface scratch.

The theoretical crazing locus accorded with the previous experimental results, except for the data near the shear yield locus in the second quadrant, which were considered to be affected by shear yielding. It was also indicated in the calculation that the shape and direction of surface scratch exert a considerable influence on the trend of biaxial crazing stress.

In [12] existing criteria for craze initiation are reviewed, and their limitations are discussed. The most obvious problem is that they are formulated simply in terms of principal stresses, making no provision for the

known effects of small inclusions and surface imperfections. To solve this problem, a new criterion is proposed, which is based on linear elastic fracture mechanics. Craze initiation is treated as a frustrated fracture process rather than a yield mechanism. Calculations show that the strain energy release rate, G_I(nasc), required to generate a typical 20 nm thick nascent craze, is less than 1 J m^{-2}. This explains why flaws less than 1 μm in length are capable of nucleating crazes at stresses of 20–30 MPa. Subsequent craze propagation is dependent upon two flow rates, one relating to fibril drawing at the craze wall and the other to shear yielding at the craze tip. Under biaxial stress, the second principal stress σ_2 affects craze tip shear yielding but not fibril drawing. This model is used in conjunction with the von Mises yield criterion to derive a new expression for the crazing stress σ_1(craze), which provides a good fit to data on visible crazes obtained by Sternstein, Ongchin and Myers in biaxial tests on cast PMMA [Sternstein SS, Ongchin L, Silverman A. Appl Polym Symp 1968;7:175; Sternstein SS, Ongchin L. Polym Prepr Am Chem Soc Div Polym Chem 1969;10:1117; Sternstein SS, Myers FA. J Macromol Sci Phys 1973;B8:539].

3. CRAZE GROWTH

Growth can be broken up into two components: (1) craze tip advancement and (2) craze thickening or widening [13]. Craze tip advancement probably occurs through the formation of more voids from the stress concentration at the tip. Craze thickening involves the drawing of craze fibrils from bulk polymer [14]. For a fibril to elongate, the polymer chains in the fibrils must experience a combination of chain scis1sion and reptation [15].

The crazing rate in polymers is dependent on several factors. Some of the known factors are stress, temperature, humidity, molecular weight, and molecular orientation. It is commonly accepted that crazing can only occur in the presence of local tensile stress. The magnitude of stress is an important factor in craze behavior. The time to craze initiation decreases with the stress increase making it a viscoelastic property like creep [6]. Also, at low-tensile stresses or strain rates, fewer crazes form, but those that do could grow to larger sizes. In contrast, in conditions of higher tensile stresses or strain rates, many smaller crazes form [6]. To illustrate the load-bearing characteristics of a craze, it has been found that crazes in PC can reach strains as high as 200% before fracture [6].

Several stress or strain based craze initiation criteria have been developed. Stemstein and Ongchin [16] produced a stress criterion based on the biaxial loading of a polymethyl methacrylate (PMMA). Their craze envelope is defined by

$$\sigma_b = A(T) - \frac{B(T)}{I_1} \qquad (1)$$

where $\sigma_b = |\sigma_1 - \sigma_2|$ is the flow stress being twice the maximum shear stress where σ_1 and σ_2 are of opposite sign. $I_1 = \sigma_1 + \sigma_2 + \sigma_3$ is the first stress invariant, and A and B are temperature-dependent constants [16]. One problem with this criterion is that the use of $|\sigma_1 - \sigma_2|$ implies the direction of maximum shear stress, but crazes form perpendicular to the maximum principal normal stress.

Gent [17] developed a craze initiation criterion based on the assumption that the dilatational stress at a flaw increases the free volume and decreases the local T_g of the material to the temperature of testing, making the stress-softened material unprotected from cavitation. Gent's model is given by

$$\frac{\sigma_c}{3} = \frac{1}{k}\left[\beta\left(T_g - T\right) + P\right] \qquad (2)$$

where: σ_c is the critical applied tensile stress, β is the hydrostatic pressure coefficient of T_g, T is the test temperature, P is the applied hydrostatic pressure, and κ is the stress concentration factor relating the applied stress to the micro-stress at the flaw tip.

Crazing has already been categorized as a viscoelastic deformation process like creep and stress relaxation involving multiple localized deformation sites instead of bulk deformation. A theory has been developed in an attempt to describe creep and stress relaxation properties as thermally activated rate processes [2]. It is possible that this theory could also apply to craze growth since similar changes in the polymer must occur in both crazing and creep, only to a smaller degree.

The theory begins with the Arrhenius equation, as shown in equation (3), which generally describes how the temperature affects the frequency of thermally activated processes, such as chemical reactions.

$$\nu = \nu_0 \exp\left(-\frac{\Delta H}{RT}\right) \qquad (3)$$

where ν is the frequency of the chemical reactions, ν_0 is a constant, ΔH is the activation energy required to overcome the potential energy barrier for a given process, R is the gas constant, and T is the absolute temperature. For crazing, the energy barrier comes from the requirement of the polymer molecules to slide past other chains (via reptation) and to undergo conformational changes.

Building on the Arrhenius equation, a model was developed to describe the effect of an applied stress on a thermally activated rate process [2]. The applied stress is believed to produce changes in the potential energy barrier in a way that decreases the height of the barrier in the direction of flow, enhancing reptation and conformational changes necessary for crazing.

The changes to the potential energy barrier are shown in fig. 3.

The Eyring equation was developed to describe the strain rate in the direction of the applied stress in a thermally activated deformation process. The Eyring equation that applies when the term va/RT is large is

$$\frac{de}{dt} \approx \frac{1}{2} e_0 \exp\left(-\frac{\Delta H - \nu\sigma}{RT}\right) \qquad (4)$$

where $\frac{de}{dt}$ is the strain rate, e_0 is a constant, v is an activation volume, ΔH, R and T are defined as above, and σ is the applied stress. This equation mathematically models the changes in the energy barrier due to an applied stress. The more contemporary criteria include effects of stress, strain, temperature, molecular weight, and entanglement density.

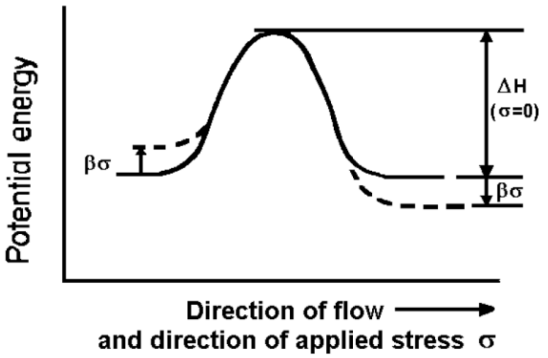

Fig.3. Effect of applied stress to the potential energy barrier of a thermally activated rate process [2].

4. EFFECT OF MOISTURE

Extensive research has been performed to determine the effect of solvent exposure on the craze behavior of polymers [9, 13, 18–20]. The time for polymer crazes to initiate decreases in the presence of some vapors or liquids. Two possible explanations for this relationship are that the small molecules of the solvent weaken the intermolecular forces of the polymer chains and the surface energy is lower in the presence of the liquid [9, 19-21]. The general conclusions for the first explanation are that the liquid diffuses into flaws and plasticizes the polymer, making it vulnerable to cavitation [22]. For the second possible explanation, the reasoning is that lowering the surface energy makes void formation easier [9].

The most widely accepted theory of craze initiation and growth in the presence of a solvent is called the meniscus instability model. It was developed by Argon and Salama [13,14,23]. The principle of meniscus instability is the phenomenon that occurs with a climbing liquid in a capillary tube. In a craze, the material in the tip is plastically deformed and acts as the liquid in the meniscus model. The surface energy of the interfaces governs the instability. The interfacial surface energy decreases if a solvent enters the craze and replaces the air, causing the instability to increase and the craze to grow at a higher rate. This explanation agrees with experimental evidence.

Craze thickening can also be explained with meniscus instability [13]. The model describes a region of material a few nanometers thick between the fibrillated and bulk polymer. A series of menisci are formed in this region from negative hydrostatic tension. This process describes the formation of surface drawn fibrils. Craze growth kinetics are related to the magnitude of the hydrostatic tension.

This study will not consider the typical organic solvents that have been frequently cited [9, 13, 18-20, 21, 22]. The assumption is that exposure to common craze accelerating solvents will be limited in application, and that their effects are already well documented. This study will concentrate on the effect of moisture on the craze behavior of polymers. Previous research has concluded that moisture produces changes in the crazing rate similar to organic solvents, but to a lesser degree [19,24, 25].

Arnold [19] studied the effect of water absorption on the strength of poly(methyl methacrylate) (PMMA). She found that the failure stress decreased after being immersed in water, similar to the effect of exposure to ethylene glycol. Another observation reported by Arnold was that craze initiation was longer for samples that were immersed in water for longer amounts of time prior to loading. Two possible reasons for this behavior are that: 1) during the long immersion times, the absorbed water blunts the flaws, or 2) the surface eventually develops compressive stresses, making it more difficult for crazes to form.

Josserand, et al. [24], studied the effect of moisture on the fracture of PMMA. They found that the diffusion of water into PMMA is governed by Fick's law, but state that the time to diffuse into the fibrils could be much faster than the time to saturate the bulk polymer since the craze fibrils have such a large surface-to-volume ratio. In their study, water behaved like a plasticizer by lowering the glass transition temperature (T_g), tensile modulus, and yield strength of the polymer. They found that the lifetime of a craze fibril immersed in water was three orders of magnitude lower than that in dry air.

Notomi et al. [25] found similar results for PS and styrene/acrylonitrile (SAN). They concluded that the absorption of moisture decreased the stress required for crazing, causing increased amounts of crazing compared to dry polymers.

5. EFFECT OF MOLECULAR WEIGHT

One of the most important factors affecting craze behavior is intermolecular entanglements. Entanglements refer to the interaction between long polymer molecules which limit chain mobility. In contrast to cross linking, no primary chemical bond exists at the entanglement point. The ability of a polymer to form entanglements depends on molecular weight. Each polymer has a critical entanglement molecular weight (M_c), below which the chains are too short to entangle. If the modulus of the rubbery plateau in a modulus/temperature plot is not a function of molecular weight, then it can be assumed that the entanglement molecular weight is also independent of the bulk molecular weight [5].

The entanglement density is defined as the number of entanglement points per unit volume. PC has a high entanglement density due to its stiff molecules containing benzene rings in the chain backbone.

Many recent studies have determined that entanglements play a dominant role in craze resistance. To form the microstructure of a craze, the polymer must undergo entanglement loss, either by chain scission or

disentanglement [7]. Ishikawa found that the critical stress to initiate crazing is directly proportional to molecular weight. He related this finding to the fact that the melt viscosity increases with increased molecular weight due to a greater amount of intermolecular interactions. He concluded that crazing involves disentanglement due to the slippage of polymer molecules from the high dilatational stresses present [5].

McLcish [7] also determined that entanglements play a role in crazing from the fact that critical molecular weights have been found below which stable crazes cannot form. These critical craze molecular weights are on the same order of magnitude as the entanglement molecular weight. The model developed by McLcish consists of a segment of a long polymer chain anchored on a growing craze fibril. As the fibril grows, it pulls on this chain segment forcing the Ions polymer chain to disentangle along its contour. The expression for this model is given below by

$$S_c \approx \sqrt{\sigma_{yd0}(T)\frac{M}{M_e}\left(\frac{\varepsilon}{\varepsilon_c}\right)^{\frac{1}{n}}\Gamma_d} \qquad (5)$$

where S_c is the bulk crazing stress, σ_{yd0} is the yield stress for molecules of entanglement molecular weight M_e, M is the molecular weight, ε_c is the critical local deformation rate, ε is the local strain rate at the critical stress, n is a scaling parameter, and Γ_d is the surface energy for a disentanglement-dominated craze. Γ_d is defined as

$$\Gamma_d = \gamma + w\frac{\varepsilon}{\varepsilon_0}\left(\frac{M}{M_e}\right)^{\frac{3}{2}} d\nu_e \qquad (6)$$

where γ is the van der Waals surface energy, w is the contribution of single entanglement length to the disentanglement dissipation, ν_c is the entanglement density, and d is the spatial separation of linked entanglements. The authors claim that, since PC has a high entanglement density, y is negligible and $S_c \approx M^{5/4}$.

Plummer and Donald [26], looked at shear deformation and crazing of PC that was aged for various amounts of time at 130°C. They defined the localized shear deformation as deformation zones (DZ). They found the following relationships:

(1) A transition from DZ's to crazing occurs with increasing temperature.

(2) Critical strain for craze initiation does not depend on aging time.

(3) The DZ/craze transition temperature is inversely proportional to aging time.

(4) The critical craze strain increases with molecular weight at a given temperature just above the transition temperature.

(5) The transition temperature is independent of molecular weight and weakly dependent on temperature in higher temperature regions.

(6) Decreasing the strain rate lowers the critical strain for craze initiation and the transition temperature.

The authors noted that the crazes in low molecular weight material became unstable at low strain rates near the T_g by forming cracks soon after initiation. They measured the craze extension ratio, λ_{crazy}, and found it to be constant along the length of the craze. They concluded that craze widening, which involves the formation and extension of fibrils, is brought about by drawing the bulk polymer instead of by fibril creep. If fibril creep occurred, then the extension ratio of the fibrils formed first would eventually be greater than the newly formed fibrils. Also, for PC, which has a high entanglement molecular weight, experimental evidence shows a molecular weight dependence of crazing. Since disentanglement is expected to depend on molecular weight while chain scission and shear flow are not, they believe that PC exhibits disentanglement-dominated craze growth.

6. MECHANICAL PROPERTIES OF CRAZED MATERIAL

The crazing literature concentrates on the initiation and growth of crazes, but is incomplete in the area of determining the effect of crazes on the mechanical properties of polymers. One obvious reason for this void is the absence of a universally accepted technique to measure the amount of crazing on a polymeric sample.

One attempt to predict the effect of crazing on the mechanical properties of polystyrene (PS) was presented by Tang and coworkers [27]. They used the finite element method (FEM) to predict the elastic modulus in the craze fibril direction (E_1), the elastic modulus perpendicular to the fibril direction (E_2), the shear modulus (G_{12}), and Poissoirs ratio (ν_{12}) of crazed PS. In their model, they could only consider uniform, low density crazes due to software limitations. Specifically, Tang, et al., found that crazed polymers have lower strength since crazes have a lower modulus and higher porosity than the undamaged bulk polymer. They found that E_1 decreased significantly, ν_{12} and G_{12} decreased slightly, and E_2 were not affected. These results show that the properties perpendicular to the crazes are most affected, which could be expected. For this reason, all of the results reported in this dissertation are in the direction perpendicular to the craze surfaces.

7. DIFFERENTIAL SCANNING CALORIMETRY

DSC is a thermal technique commonly used to measure transitions in polymers like the glass transition temperature and melting temperature [28]. In its most common uses, polycarbonate is an amorphous thermoplastic with a glass transition temperature around 145°C.

The free volume theories used to explain the physical aging process of polymers indicate that when aging occurs, the free volume in the polymer decreases. With lower free volume there is a decrease in molecular mobility which leads to changes in mechanical properties of the polymer and an increase in the glass transition temperature [8, 29]. This occurs because the polymer needs to reach a higher temperature to produce large scale molecular motion when less free volume is available for chain movement. Thus, changes in the T_g provide

important information for the detection of physical aging, and DSC was used to measure shifts in the T_g.

A general description of the DSC technique is given by considering the meaning of each of the three words: 1) Calorimetry implies the measurement of heat capacity (C_p); 2) Scanning implies that a temperature range is being scanned, making sure to include the desired transition temperature; 3) Differential describes the process since it looks at the difference between the heat capacity of an empty pan and the heat capacity of a pan/sample combination [30].

The glass transition is seen as a characteristic jump in the heat capacity. This is because the heat capacity in the rubbery state (above T_g) is larger than the heat capacity in the glassy state (below T_g). The rubber has a larger heat capacity since it includes rotational, vibrational and conformational contributions while the glass heat capacity only includes contributions from rotations and vibrations (fig. 4). The absence of conformational energy in the glass is due to the fact that below the glass transition, the conformational changes of the polymer are negligible since the energy level is too low to permit the cooperative motion of a large number of chain segments [30].

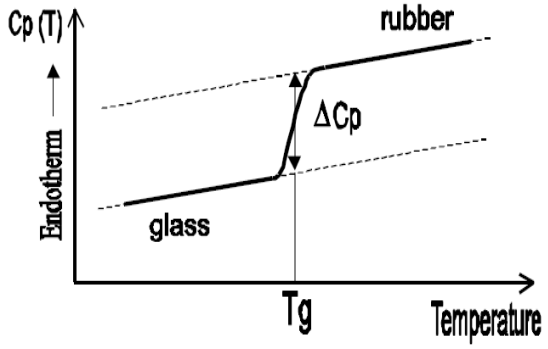

Fig. 4. Conceptual graph of DSC scan.

8. INITIALIZATION CRAZY CENTERS BY THE USE OF ELECTRIC DISCHARGE PLASMA

The aim of this work was to investigate how the crystallization of polymer–piezoelectric ceramic matrix composites under the action of the electric discharge plasma [31]. For this purpose, we used the electric discharge that arises in an air medium bounded by insulators, i.e., in the metal–insulator–gas medium–composite–metal structure, and allows one to modify uniformly the composite throughout the volume. Taking into account that the development of this discharge is attended by the formation of accelerated electrons and ions, the generation of recombination radiation, the appearance of gaseous products, and electron–ion surface effects, it is necessary to optimize the conditions for the crystallization of composites under the action of the electric discharge plasma.

The crystallization under the action of the plasma of the electric discharge initiated by a high sinusoidal voltage was performed in several stages. At the first stage, the composite was heated to the melting temperature. At the second stage, the composite was held under the discharge at this temperature for 5–10 min. At the third stage, the composite was cooled (in the presence of the discharge) to the crystallization temperature of the polymer phase at a rate of 0.5–4.0 K/min in order to vary controllably the chemical and physical structures of the polymer matrix.

We assume that method of the action of the plasma of the electric discharge creates more uniform distribution of crazes in polymer. So, our method has advantage over other methods.

5. CONCLUSION

There have been presented in paper a literature review of craze initiation and growth of crazes in polymer materials including composite one. There is a discussion concerning of mechanical properties of crazed material in paper. A proposed idea about new method of initialization crazy centers by the use of electric discharge plasma is discussed.

ASKNOWLEDGEMENTS

This work was supported by the Science Development Foundation under the President of the Republic of Azerbaijan – Grant № EİF-BGM-2-BRFTF-1-2012/2013-07/01/1-M-06.

[1] *H.H. Kausch.* Crazing in Polymers. Editor: Springer-Verlag Berlin Heidelberg NewYork Tokyo 1983.

[2] *Stephen Brett Clay*. Characterization of crazing properties of polycarbonate. Dissertation. August 15, 2000, Blacksburg, Virginia.

[3] *O.V. Arjakova, A.A. Dolgova, L.M. Yarisheva, A.L. Bolinskiy, N.F.Bakeev*. Forming stabile open porous structure in high density polystyrene on crazing mechanism. Perspective materials 2011 №1, pp.39-46.

[4] *O.V. Arzhakova, A.A. Dolgova, I.V. Chernov, L.M. Yarysheva, A.L. Volvnskii, N.F. Bakeev*. The Effect of Preliminary Orientation of Polymers via Tensile Drawing at Elevated Temperature on Solvent Crazing. High-molecular compounds, Series A, 2007, v. 49, M 8, pp. 1502-1509.

[5] *M. Ishikawa, Y. Sato, and H. Higuchi,* "Effect of intermolecular interactions on the plastic deformation of glassy polymers," *Polymer,* 37, n7, 1177 (1996).

[6] *R.P. Kambour,* "A review of crazing and fracture in thermoplastics," Journal of Polymer Science: Macromolecular Reviews, 1', 1 (1973).

[7] *T.C.B. McLeish, C.J.G. Plummer and A.M. Donald.* "Crazing by disentanglement: non-diffusive reptation," *Polymer,* 30, 1651 (1989).

[8] *L.H. Sperling*. Introduction to Physical Polymer Science, 2nd edition, John Wiley & Sons, Inc., New York (1992).

[9] *J.C. Arnold,* "Environmental stress crack initiation in glassy polymers," Trends in Polymer Science (UK), 4, nl2, 403 (1996).

[10] *M. Ishikawa and H. Takahashi,* "Crazing mechanism based on plastic instability," Journal of Materials Science, 26, 1295 (1991).

[11] *M. Kawagoe, M. Kitagawa*. On criteria for craze initiation in glassy polymers. Journal of Materials Science. 1988, V. 23, Is. 11, pp 3927-3932.

[12] *C.B. Bucknall*. New criterion for craze initiation. Polymer**,** 2007, V. 48, Is. 4, pp. 1030–1041.

[13] *A.L. Volynskii and N.F. Bakeev,* Solvent Crazing of Polymers, Elsevier, NY (1995).

[14] *G.J. Salomons, M.A. Singh, T. Bardouille, W.A. Foran, and M.S. Capel,* "Small-angle x-ray scattering study of craze formation and dynamics in thermoplastics," Macromolecules, 32, 1264 (1999).

[15] *H.Z.Y. Han, T.C.B. McLeish, R.A. Duckett, N.J. Ward, A.F. Johnson, A.M. Donald and M. Butler*. "Experimental and theoretical studies of the molecular motions in polymer crazing. 1. Tube model", Macromolecules, 31, 1348 (1998).

[16] *S.S. Sternstein and L. Ongchin.* "Yield criteria for plastic deformation of glassy high polymers in general stress fields," Polymer Preprints, American Chemical Society, Division of Polymer Chemistry, 10, n2, 1117 (1969).

[17] *A.N. Gent.* "Hypothetical mechanism of crazing in glassy plastics;' Journal of Materials Science, 5, 925 (1970).

[18] *J.C. Arnold and J.E. Taylor*. "Improved thermodynamic approach for predicting the ESC behavior of polycarbonate in binary liquid mixtures," Journal of Applied Polymer Science (USA), 71, nl3,2155 (1999)

[19] *J.C. Arnold.* "The effects of diffusion on environmental stress crack initiation in PMMA," *Journal of Materials Science (UK),* 33, n21, 5193 (1998).

[20] *X. Qin and W.V. Chang*. 'The role of interfacial free energy in wettability, solubility, and solvent crazing of some polymeric solids " Journal of Adhesion Science and Technology (Netherlands), 10, nlO, 963 (1996).

[21] *M.Kotoul.*"Micromechanical and thermodynamical aspects of environmental crazing," Journal of Materials Science (UK), 31, nl3, 3333 (1996).

[22] *K. Iisaka, M. Hayama, and A. Fukami.* "Dependence of solvent crazing in bisphenol-A polycarbonate on molecular weight of organic liquids," Journal ofMacromolecular Science - Physics, B27, n4, 385 (1988).

[23] *J. Liu and A.F. Yee.* "Effect of local conformational transition on craze initiation in polyestercarbonates containing cyclohexylene linkages," Macromolecules, 33, 1338 (2000).

[24] *L. Josserand, R. Schirrer, and P. Davies*. "influence of water on crack propagation in polymethyl methacrylate: craze stress and craze fibril lifetime," Journal of Materials Science$_9$3Q$_9$ 1772(1995).

[25] *M. Notomi, K. Kishimoto, T. Shibuya, T. Koizumi*. "Effects of moisture absorption on fracture behaviors of acrylonitrile-butadiene-styrene resin," Journal of Applied Polymer Science, 72, 435 (1999).

[26] *C.J.G. Plummer, and A.M. Donald.* "The deformation behavior of polyethersulfone and polycarbonate," Journal of Polymer Science: Part B: Polymer Physics, 27, 325 (1989).

[27] *C.Y. Tang, L.C. Chan, M. Jie, and C.H. Yu.* "Prediction of the effect of craze damage on apparent elastic properties of polystyrene by FEM," Key Engineering Materials (Switzerland), 145-149**,** nl, 249 (1998).

[28] *D.A. Skoog and J.J. Leary.* Principles of Instrumental Analysis, 4 eel., Harcourt Brace College Publishers, NY, 568 (1992)

[29] *P.C. Hiemenz.* Polymer Chemistry: The Basic Concepts, Marcel Dekker, Inc. NY (1984).

[30] *H. Marand.* Physical Chemistry of Polymers class notes (2000).

[31] *M.A. Kurbanov, I.S. Sultanakhmedova, E.A. Kerimov, Kh.S. Aliev, G.G. Alieva, G.M. Geidarova.* Plasma Crystallization of Polymer–Ferroelectric/Piezoelectric Ceramic Composites and Their Piezoelectric Properties. Physics of the Solid State, 2009, Vol. 51, No. 6, pp.1223–1230.

Recevied: 04.12.2013

VORTEX LATTICE IN TWO-BAND SUPERCONDUCTOR LiFeAs USING GINZBURG-LANDAU THEORY

I.N. ASKERZADE[1,2], R. ERYIĞIT[1], N. GUCLU[3], M.E. ÇELIK[1], A.H. ZIROĞLU[1]

Computer Engineering Department of Engineering Faculty, Ankara University, Golbaşı 50.yıl campus Bahçelievler, 06830, Ankara, Turkey
Institute of Physics Azerbaijan National Academy of Science, Baku Azerbaijan
Necmettin Erbakan University, Physics Education Department, Konya, Turkey
e-mail: imasker@eng.ankara.edu.tr

Numerical modeling of vortex lattice in external magnetic field in two-band superconductor using modified Ginsburg-Landau (GL) theory is conducted. Results of simulation experiments for a two-band superconducting films *LiFeAs* near the critical temperature in perpendicular magnetic field are presented and it was shown quasi-hexagonal character of vortex lattice.

Keywords: two-band superconductors, nucleation of vortices, Ginsburg-Landau theory, modified Euler method
PACS: 74.25.Qt, 74.25.Sv I

1. INTRODUCTION

The discovery of superconductivity in Fe-based compounds initiated new period of investigations. In study [1], authors discovered superconductivity in LaOFeP with the critical temperature T_c=4K. The same group of researchers found superconductivity in compound $LaO_{1-x}F_xFeAs$ transition at temperature reach the 26 K [2]. After this a series of oxypnictides LaOMPn, where (M=Mn,Fe,Co,Ni,) and (Pn=P,As,Sb) were synthesized. The critical temperature T_c reached a saturation value of 56K in $SmO_{1-x}F_xFeAs$ [3]. Furthermore, it was shown that $BaFe_2As_2$ non-oxyde compound with antiferromagnetic ordering of Fe spins also becomes superconducting at T_c=38K under partial substitution of Ba by K [4], [5]. Another class of Fe-based superconductors is the type 111 compounds, for example LiFeAs [6] and NaFeAs [7]. Fe-based superconductors of the type 11 is the FeSe [8], which critical temperature T_c=8K. Superconductivity in oxypnictides occurs in Fe planes (see [9], [10]).

Similar to cuprates, Fe-based compounds becomes superconducting on doping of parent antiferromagnetic state. As mentioned in [11], a layered crystal structure of Fe based compounds similar to the high-T_c cuprates. However, significant discrepancies have been observed between the Fe-based superconductors and cuprate superconductors. For example, d-wave superconductivity was realized in cuprate compounds, but an s±-type order parameters has been proposed for Fe-based superconductors [12]. Another peculiarity of Fe-based compounds related with multiband character of superconducting state [13], [14]. One of widely investigated Fe-based superconductor is the LiFeAs. Unusual superconductivity in these compounds is related with two distinct energy gap associated with different part of the Fermi surface. The smaller gap (Δ_1 =1.5 meV) originates from hole like carriers residing on two cylindrical Fermi surface sheets, while the strong gap (Δ_2 =2.5 meV) originates from the electron like carriers [15], [16]. Two-band characteristic of the superconducting state in LiFeAs is clearly evident in the recently performed specific heat measurement [17] and from first principle calculations [18].

The very recently investigation of vortices in LiFeAs using scanning tunneling spectroscopy was conducted in [19]. Zero-field measurements confirms existence two superconducting gap in this compound. Image of vortices in a wide field range from 0.1 T to 11T obtained using tunneling conductance at the Fermi energy. A quasihexagonal vortex lattice at low field contains domain boundaries which consist of alternating vortices with unusual coordination number of 5 and 7. However, theoretical analysis of vortex lattice in two-band superconductor LiFeAs was not conducted. In the present study, the vortex lattice structure in external magnetic field in the framework of a two-band GL equations is conducted and obtained results applied to LiFeAs compound. Previously, time independent two-band GL equations were successfully used to study the physical properties of recently discovered superconductors such as magnesium diboride *(MgB2)* [20, 21] and nonmagnetic borocarbide compounds *(Y(Lu)Ni2B2C)* [22,23]. Firstly we will drive time-dependent GL equations for two-band superconductors. Secondly we apply these equations for numerical modeling for vortex nucleation in the case thin superconducting film of two-band superconductor *LiFeAs* with perpendicular external magnetic field. We could use the modified forward Euler method for numerical experiments. Finally, a conclusion remarks will be made.

2. TIME-DEPENDENT GL EQUATIONS FOR TWO-BAND SUPERCONDUCTORS

The GL free energy functional for an isotropic two-band superconductor can be written as follows [20-23]:

$$F_{SC} = \int d^3 r (F_1 + F_{12} + F_2 + H^2/8\pi) \tag{1}$$

where

$$F_i = \frac{\hbar^2}{4m_i}\left|\left(\nabla - \frac{2\pi i\vec{A}}{\Phi_0}\right)\Psi_i\right|^2 + \alpha_i(T)\Psi_i^2 + \beta_i\Psi_i^2/2 \quad (2)$$

$$F_{12} = \varepsilon(\Psi_1^*\Psi_2 + c.c.) + \varepsilon_1\left\{\left(\nabla + \frac{2\pi i\vec{A}}{\Phi_0}\right)\Psi_1^*\left(\nabla - \frac{2\pi i\vec{A}}{\Phi_0}\right)\Psi_2 + c.c.\right\} \quad (3)$$

mi are the masses of electrons belonging to different bands (i = 1, 2); $\alpha i = \gamma i(T - Tci)$ are the quantities linearly dependent on the temperature; βi and γi are constant coefficients; ε and ε1 describe the interaction between the band order parameters and their gradients, respectively; H is the external magnetic field; and Φ_0 is the magnetic flux quantum. In Eqs. (1) and (2), the order parameters $\Psi_{1,2}$ are assumed to be slowly varying in space. Minimization procedure of the free-energy functional yields the GL equations describing the two-band superconductors. For an isotropic superconductor in the case (not limiting the generality) of A = (0, Hx, 0), the time-independent GL equations take the following form:

$$-\frac{\hbar^2}{4m_1}\left(\frac{d^2}{dx^2} - \frac{x^2}{l_s^4}\right)\Psi_1 + \alpha_1(T)\Psi_1 + \varepsilon\Psi_2 + \varepsilon_1\left(\frac{d^2}{dx^2} - \frac{x^2}{l_s^4}\right)\Psi_2 + \beta_1\Psi_1^3 = 0, \quad (4a)$$

$$-\frac{\hbar^2}{4m_2}\left(\frac{d^2}{dx^2} - \frac{x^2}{l_s^4}\right)\Psi_2 + \alpha_2(T)\Psi_2 + \varepsilon\Psi_1 + \varepsilon_1\left(\frac{d^2}{dx^2} - \frac{x^2}{l_s^4}\right)\Psi_1 + \beta_2\Psi_2^3 = 0 \quad (4b)$$

where $l_s^{-2} = \frac{\hbar c}{2eH}$ is the so-called magnetic length. In the general case the signs of the parameters of interband interaction ε and ε_1 in Eqs. (4a) and (4b) can be arbitrary. These signs are determined by the microscopic nature of the interaction of electrons belonging to different bands. If the interband interaction vanishes then Eqs. (4a) and (4b) transform into the usual GL equations with the critical temperatures Tc1 and Tc2. In the general case (irrespective of the sign of ε), the superconducting transition takes place at a temperature Tc, which is higher than both Tc1 and Tc2 and is determined by the following equation [20–23]:

$$(T_c - T_{c1})(T_c - T_{c2}) = \frac{\varepsilon^2}{\gamma_1\gamma_2}, \quad (5)$$

Time-dependent equations in two-band Ginzburg-Landau theory can be obtained from Eqs. (1-3) in analogical way to [24]:

$$\Gamma_1\left(\frac{\partial}{\partial t} + i\frac{2e}{\hbar}\phi\right)\Psi_1 = -\frac{\delta F}{\delta\Psi_1^*} \quad (6a)$$

$$\Gamma_2\left(\frac{\partial}{\partial t} + i\frac{2e}{\hbar}\phi\right)\Psi_2 = -\frac{\delta F}{\delta\Psi_2^*} \quad (6b)$$

$$\sigma_n\left(\frac{\partial A}{\partial t} + \nabla\phi\right) = -\frac{1}{2}\frac{\delta F}{\delta A} \quad (6c)$$

Here we use notations similar to [24]. In Eqs. (6) φ means electrical scalar potential , $\Gamma_{1,2}$ -relaxation time of order parameters $\Psi_{1,2}$, σ_n-conductivity of sample in two-band case. Choosing corresponding gauge invariance, we can eliminate scalar potential from system of equations (6) [24]. Under such calibration and magnetic field in form, $\vec{H} = (0,0,H)$ without any restriction of generality, time-dependent equations in two-band Ginzburg-Landau theory can be written as

$$\Gamma_1\frac{\partial\Psi_1}{\partial t} = -\frac{\hbar^2}{4m_1}\left(\frac{d^2}{dx^2} - \frac{x^2}{l_s^4}\right)\Psi_1 + \alpha_1(T)\Psi_1 + \varepsilon\Psi_2 + \varepsilon_1\left(\frac{d^2}{dx^2} - \frac{x^2}{l_s^4}\right)\Psi_2 + \beta_1\Psi_1^3 = 0, \quad (7a)$$

$$\Gamma_2\frac{\partial\Psi_2}{\partial t} = -\frac{\hbar^2}{4m_2}\left(\frac{d^2}{dx^2} - \frac{x^2}{l_s^4}\right)\Psi_2 + \alpha_2(T)\Psi_2 + \varepsilon\Psi_1 + \varepsilon_1\left(\frac{d^2}{dx^2} - \frac{x^2}{l_s^4}\right)\Psi_1 + \beta_2\Psi_2^3 = 0, \quad (7b)$$

$$\sigma_n\left(\frac{\partial\vec{A}}{\partial t} - \nabla\phi\right) = -rot\vec{A} + \frac{2\pi}{\Phi_0}\left\{\frac{\hbar^2}{4m_1}n_1(T)\left(\frac{d\varphi_1}{dr} - \frac{2\pi A}{\Phi_0}\right) + \varepsilon_1(n_1(T)n_2(T))^{0.5}\cos(\varphi_1 - \varphi_2) + \frac{\hbar^2}{4m_2}n_2(T)\left(\frac{d\varphi_2}{dr} - \frac{2\pi A}{\Phi_0}\right)\right\} \quad (7c)$$

where $\phi_{1,2}(\vec{r})$ is phase of order parameters $\Psi_{1,2}(\vec{r}) = |\Psi_{1,2}| \exp(i\phi_{1,2})$, $n_{1,2}(T) = 2|\Psi_{1,2}|^2$ is density of superconducting electrons in different bands, expressions for whichs are presented in [20–23] with so-called natural boundary conditions

$$\left\{ \frac{1}{4m_1}(\nabla - \frac{2\pi i\vec{A}}{\Phi_0})\Psi_1 + \varepsilon_1(\nabla - \frac{2\pi i\vec{A}}{\Phi_0})\Psi_2 \right\} \vec{n} = 0, \quad (8a)$$

$$\left\{ \frac{1}{4m_2}(\nabla - \frac{2\pi i\vec{A}}{\Phi_0})\Psi_2 + \varepsilon_1(\nabla - \frac{2\pi i\vec{A}}{\Phi_0})\Psi_1 \right\} \vec{n} = 0, \quad (8b)$$

$$(\vec{n} \times \vec{A}) \times \vec{n} = \vec{H}_0 \times \vec{n} \quad (8c)$$

First two conditions correspond to absence of supercurrent through boundary of two-band superconductor, third condition corresponds to the contiunity of normal component of magnetic field to the boundary superconductor-vacuum.

In this study we introduce unconventional scales to non-dimensionalize the time-dependent two-band G-L system of equations. As shown in [20–23], temperature dependence of some physical quantities becomes nonlinear in contrast to single-band G-L theory. It is well known that, G-L parameter κ for single-band superconductors is temperature independent, while in two-band G-L theory κ grows with decreasing of temperature [20–23]. This implies about possibility changing of type of superconductivity with lowering of temperature. It means that dynamics of order parameters in two-band superconductors differs from those of in single-band superconductors.

3. APPLİCATİON OF TİME-DEPENDENT TWO-BAND GL EQUATİONS TO THİN SUPERCONDUCTİNG FİLM

We consider a finite homogeneous film of a two-band superconductor of uniform thickness, subject to a constant magnetic field. We also consider that the superconductor is rectangular in shape. In this case our two-band GL model becomes two-dimensional [20–23]. The order parameters Ψ_1 and Ψ_2 varies in the plane of the film, and vector potential **A** has only two nonzero components, which lie in the plane of the film. Therefore, we identify the compuational domain of the superconductor with a rectangular region $\Omega \in R^2$, denoting the Cartesian coordinates by *x* and *y*, and the *x*- and *y*- components of the vector potential by *A(x,y)* and *B(x,y),* recpectively. Before modeling we use so-called bond variables [25] for the discretization of time-dependent two-band G-L equations

$$W(x,y) = \exp(i\kappa \int^{x} A(\zeta, y)d\zeta),$$

$$V(x,y) = \exp(i\kappa \int^{y} B(x,\eta)d\eta) \quad (9)$$

Such variables make obtained discretized equations gauge-invariant. For spatially discetization we use forward Euler method [26]. In this method we begin with partitioning the computational domain $\Omega = [0, N_{xp}] \times [0, N_{yp}]$ into two subdomains, denoted by Ω_{2n} and Ω_{2n+1} such that

$$\Omega_{2n} = \Omega \,|_{i+j=2n} \text{ and } \Omega_{2n+1} = \Omega \,|_{i+j=2n+1} \quad (10)$$

For $i = 0,.....; N_{xp}$, $j = 0,.....; N_{yp}$, where $N_{xp} = N_x + 1$, $N_{yp} = N_y + 1$.

For numerical calculations in two-band GL theory we assume that the size of superconducting film is $40\lambda \times 40\lambda$, where λ London penetration depth of external magnetic field on superconductor [20–23]:

$$\lambda^{-2}(T) = \frac{4\pi e^2}{c^2}\left(\frac{n_1(T)}{m_1} + 2\varepsilon_1(n_1(T)n_2(T))^{0.5} + \frac{n_2(T)}{m_2}\right) \quad (11)$$

Under modeling we also introduce another dimensionless parameters

$$\vec{r}' = \frac{\vec{r}}{\lambda}; \Psi'_{1,2} = \frac{\Psi_{1,2}}{\Psi_{(1,2)0}}; \vec{A} = \frac{\vec{A}}{\lambda H_c\sqrt{2}}; F'(\Psi'_{1,2}, A') = \frac{F(\Psi_{1,2}, A)}{\alpha_0^2|\Psi_{1,0}|^2 + \alpha_1^2|\Psi_{2,0}|^2} \quad (12)$$

Expressions for $\Psi_{(1,2)0}$, and for thermodynamic magnetic field *Hc* are presented in [20–23]. The calculations were performed for the following values of parameters: T_c = 18 K; *T*c1 =4.6 K; *Tc*2 = 11.55 K, $\frac{\varepsilon^2}{\gamma_1\gamma_2 T_c^2} = 0.175$, $\varepsilon_1 = 0.0976$, $\frac{\gamma_1 m_1}{\gamma_2 m_2} = 0.333$. These parameters were used for the calculation of angular dependence of upper critical field of two-band superconductor LiFeAs [26].

For solving of corresponding discretized GL equations we will use method of adaptive grid [27]. Results of numerical modelling presented in Fig. 1. We assume that the sample, which is initially in a perfect superconducting state, is cooled through T_c in the absence of applied magnetic field, and then a magnetic field of an appropriate strenght is suddenly turned out. Mathematically it means that, the initial state is achieved by letting $|\Psi'_{1,2}(\vec{x})| = 1$, $A_0(\vec{x}) = 0$ for all $\vec{x} \in \Omega$.

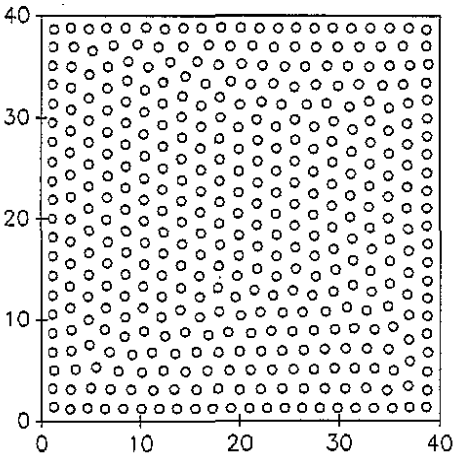

Fig. 1. A quasi-hexagonal vortex lattice for two-band superconductor LiFeAs (numerical result in this study, for experimental data see [19])

In Figure 1, we present a a contour plot of superconducting electrons. GL parameter for sample is the $\kappa = 5$. We can observe a partial hexagonal pattern , yet we do not observe the physically exact hexagonal pattern, as expected of homogeneous samples with uniform thickness. In some places of vortex lattice (Fig.1) coordination number chamges as 5 or 7 instead exact hexagonal case 6. Similar results obtained very recently in experimental study for two-band superconductor LiFeAs [19] Calculations also confirms the existence of Meissner state in thin film of two-band superconductor. It means that at fixed Ginzburg-Landau parameter κ and external magnetic field $H < H_{c1}$ no nucleation of vortexes of external magnetic field.

In the end of this paragraph it is useful to note about magnetic field distribution of vortex in two-band superconductors. As shown in [28] structure of magnetic field in section of vortex in two-band superconductor has nonsymmetric angular character. As result their interaction force between them and total energy of superconductor with such vortexes differs from single band one. In high density vortex lattice effects of influence of nonsymmetric angular dependence becomes crusial. Detail analysis of influence of asymmetric character of sectional magnetic field distribution on the parameters of hexagonal vortex pattern is the object of future investigations.

4. CONCLUSIONS

In this study we obtain time-dependent GL equations taking into account two-band character of the superconducting state. Furthermore, we perform numerical modeling of vortex lattice structure in external magnetic field in two-band superconducting films LiFeAs using GL theory. It was shown that the vortex lattice configuration in the mixed state depends upon initial state of the sample and that the system does not seem to yield hexagonal pattern for finite size homogeneous samples of uniform thickness with the natural boundary conditions. On the other hand, the time-dependent two-band GL equations lead to the expected quasi-hexagonal structure.

ACKNOWLEDGEMENTS

This work partially was supported by TUBITAK research project 110T748.

[1] *Y. Kamihara,* et al, J.Am. Chem.Soc., 128(2006)10012.
[2] *Y. Kamihara, T. Watanabe, M. Nirano, H. Hosono,* J.Am. Chem.Soc., 130(2008)3296
[3] *Z-A Ren, W. Lu, J. Yang, W. Yi,* et al, Chin.Phys.Lett.25(2008)2215
[4] *M. Rotter, M. Tegel, D. Johrendt*, Phys.Rev.Lett. 101(2008)107006
[5] *R. Prozorov, N. Ni, M.A. Tanatar,* et al Phys Rev B78(2008)224506
[6] *XC Wang, QQ Liu, YX Lv* et al , Solid State Commun. 148(2008)538
[7] *CV Chu, B. Lorentz,* Physica C,469(2009)385
[8] *F-CHu, J-Y Luo, K-W Yeh* et al, Proc. Natl. Acad. Sci.USA 105(2008)14262
[9] *A.L. Ivanovskii,* Uspekhi Fiz. Nauk, 178(2008)1273
[10] *MV Sadovski,* Uspekhi Fiz. Nauk, 178(2008)1243
[11] *ZA Ren, ZXZhao,* Adv.Mater. 21(2009)4584
[12] *T. Hanaguri, S. Niitaka, K. Kuroki, H. Takagi,* Science 328(2010)474
[13] *V.M. Pudalov* et al, Uspekhi Fiz. Nauk,181 (2011)672
[14] *I.N. Askerzade,* Unconventional Superconductors: anisotropy and multiband effects, Springer, 2012, 177 p.
[15] *K. Sasmal, B. Lv, Z. Tang,* et al Phys Rev B81(2010)144512
[16] *SVBorisenko,* et al Phys. Rev. Lett. 105,(2010) 067002
[17] *F. Wei, F. Chen, K. Sasmal* et al Phys RevB81(2010)134527
[18] *IR Shein, AI Ivanovskii,* Solid State Commun. 150(2010)152
[19] *T. Hanaguri, K. Kitagawa, K. Matsubayashi,* et al, Phys Rev B85(2012)214505
[20] *I.N. Askerzade, A. Gencer* et al , Supercond. Sci. Technol. **15**, L13(2002).
[21] *N. Askerzade, A. Gencer,* Solid State Commun. **123**, 63 (2002).
[22] *N. Askerzade,* JETP Letters 81, 583 (2005).
[23] *N. Askerzade,* Physics Uspekhi 49, 1003 (2006).
[24] *I. Shcmid* ,Phys. Kondens. Matter,v.5, p.302(1966)
[25] *M.K. Kwong, H.G. Kaper,* J.Comput. Phys. v.119.p.120(1995).
[26] *I.N. Askerzade, R.T.Tagiyeva,* Supercond. Sci. Technol. **25**, 095007(2012).
[27] *J.F. Thompson,* et al, Numerical Grid Generation, Elsevier.New York(1985).
[28] *I.N. Askerzade. B. Tanata,* Communications in Theoretical Physics. v.51.p.563 (2009)

Recevied: 07.11.2013

COMPOSITE DIELECTRIC PROPERTIES WITH NANOADDITIONS OF ALUMINUM PARTICLES

E.M. GODJAYEV, H.R. AHMEDOVA, S.I. SAFAROVA, S.S. OSMANOVA
Azerbaijan Technic University
G. Javid str, 25, Baku
geldar-04@mail.ru

The results of experimental investigation of temperature frequency dependences of dielectric constant and dielectric losses of composites PE+x·vol% $TlInSe_2$ ($1 \le x \le 10$) in temperature interval 300-450K and frequency one 25Hz-1MHz are given in work.The influences of aluminum nanoparticles on composite dielectric properties 90·vol%PE+7·vol%$TlInSe_2$+3·vol%Al; 80·vol%PE+10·vol%$TlInSe_2$+10·vol%Al; 90·vol%PE+3·vol%$TlInSe_2$+7·vol%Al are investigated.

Keywords: aluminum nanoaddition, dielectric constant, composites PE+x·vol%$TlInSe_2$
PACS: 72.80.Tm, 77.22.Ch, 72.20.−i, 61.72.−y 1

INTRODUCTION

Introduction into crystallizing polyolefines of different disperse fillers in definite quantities can lead to the change of permolecular structure, crystallinity, macro-molecule orientation degree, polymer defect structure. As a result their electro-active (electret, pieso-electric, antistatic) dielectric and electro-physical, sensor and other properties have the essential changes [1-4].

Moreover, it is expected the decrease of spherulite sizes for polyethylene, the change of crystallinity and crystallite sizes, formation of different functional groups and permolecular formations. The improvement of electro-active properties of polyethylene of low density and high one (PELD and PEHD) at introducing of fillers is mainly connected with two circumstances: filler particles play the role of structure formation center and polymer frontier layer filler has the special structure of saturation by trap centers with different values of activation energy in which electrons stabilize [3].

It is necessary to note that in the dependence on nature, size, form, distribution character of filler, obtained polymer composition can be current-conducting, antistatic or dielectric one.

By these reasons the conclusions of different authors differ relatively revealing nature of these or that electro-active properties of composites at polyolephine filling by different piezo-fillers [1-11].

It is known that triple semiconductor compound $TlInSe_2$ has high coefficient of photo-and tensosensitivity and switching properties with memory [9-11]. The composites on its base have the well electret properties [12].

However, their dielectric, electro-physical, physic-mechanical and peculiarities of interphase phenomena in the system of polymer-semiconductor are little-studied. The study of these questions would serve the formation of new electro-active composite materials with controlled properties.

The aim of the given work is the study of dielectric properties of compositions on the base of PEHD with semiconductor filler $TlInSe_2$ (ΔE = 1,2eV). The compound $TlInSe_2$ has the essential flexibility, tensile strength and high tensosensitivity. The specific electric resistance of $TlInSe_2$ is 10^9—10^{11} Om·m [7].

EXPERIMENTAL PART

The samples are obtained by hot pressing from mixture powder and $TlInSe_2$ filler with dispersivity up to 50 μm. The polymer and filler powders are mixed on laboratory mill at room temperature, then the samples of thickness 150-200 μm between two Al foils are obtained from mixture by hot pressing (at 10^7 Pa, temperature 443 and 473K with further hardening at 273K). The calculation of ε dielectric constant values is carried out by formulae from [13] as statistic mixture:

$$\varepsilon = \varepsilon_2 \left[1 + \frac{\nu}{\frac{(1-\nu)}{3} + \frac{\varepsilon_2}{(\varepsilon_1 - \varepsilon_2)}} \right] \qquad (1)$$

where ε_1 and ε_2 are dielectric constant values of components of polymer and filler correspondingly, ν is filler part in mixture. We obtain ε value [7] at ε_1 = 14,1 for filler and ε_2 = 2,3 for PE. The loss tangent $tg\delta$ and dielectric constant are measured by the bridge E7-8 at heat rate $\beta \sim$ 2,5K/min. The errors at calculation ε and $tg\delta$ are 5 and 12% correspondingly.

RESULTS AND THEIR DISCUSSION

The obtained experimental results are given on fig.1a. As it is followed from fig.1a with increase of $TlInSe_2$ additions in composite content ε increases, but change character of dielectric constant in investigated composites is similar.

It is seen that with increase of $TlInSe_2$ content in compositions on PE base ε value increases and the some additional increase of its values is observed on dependence $\varepsilon(T)$ (fig.1a) at polymer softening temperature.

The calculations by formulae (1) of ε values are given in table. From the table it is seen that results (fig.1a) satisfactory agreeing with experiment are obtained at low values of filler degree. At relatively high values of filler degree in calculation and experimental data of dielectric constant ε the some divergence is observed. Such

divergence of calculation and experimental values ε of compositions can be connected with both dispersivity and possibility of intralayer polarization in heterogeneous composite systems.

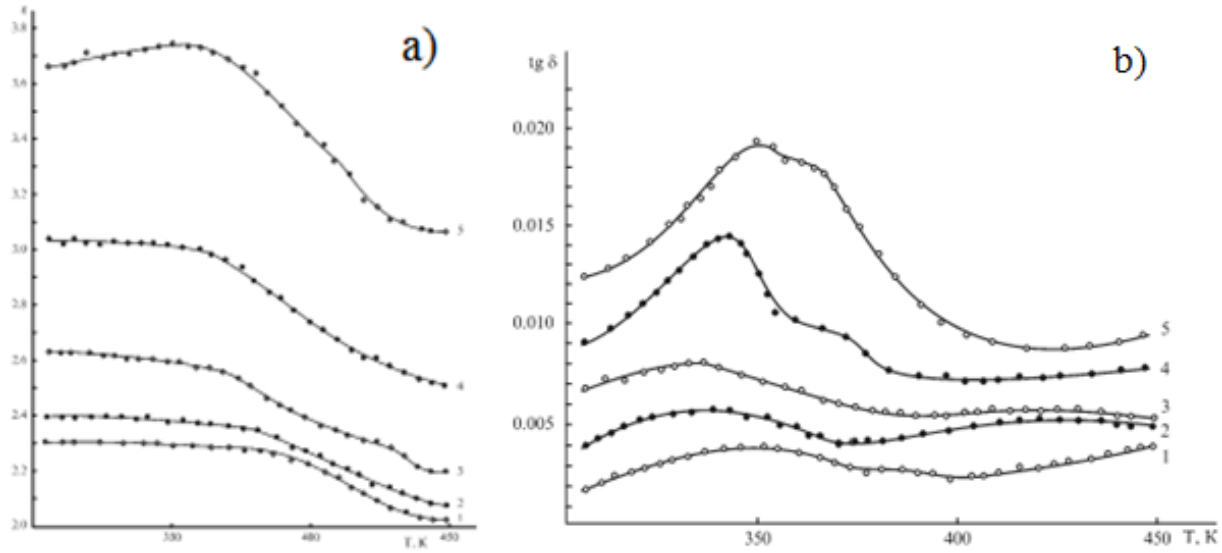

Fig.1. The temperature dependences: a) dielectric constant $\varepsilon(T)$ and b) dielectric losses $tg\delta$ (T) of PE/ $TlInSe_2$ composites at filler content, %; 1-0; 2-1; 3-3; 4-5; 5-10

Table.

$TlInSe_2$	0%	1%	3%	5%	10%
ε_{pe}^{n}	2.2	2.2	2.33	2.42	2.65
ε_{pe}^{eks}	2.1	2.3	2.6	2.85	3.6

The temperature dependence tgδ*(T)* of compositions on PE base at different filler content $TlInSe_2$ are given on fig.1b. From these data it is seen that with increase of $TlInSe_2$ content in compositions up to 10% vol. in temperature interval 350-420K the dielectric loss maximums which can be connected by melting of polymer matrix in composite are observed. Besides dielectric losses have two maximums: the first is in temperature interval 320-345K and the second one is in temperature interval at 350-380K for compositions on PE base (fig.1b). Moreover, for compositions on PE base the second maximum of dielectric losses is weakly expressed. The increase of second peak intensity on dependences tgδ *(T*) shows that dielectric losses at high temperatures are caused by essentially charge movement in filler, and also by accumulation in interphase boundary and decay in tgδ values is observed after exhaustion.

Further, the insignificant increase tgδ at high temperatures is result of conducting increase of general system after polymer matrix melting. The frequency dependences of dielectric constant of compositions PE+$TlInSe_2$ are investigated. The investigation results are given on fig.2a. In interval 0-1MHz as it is followed from the picture, the maximum at frequency 100kHz is observed for composites 3 vol.% and 10 vol.% $TlInSe_2$ on curves ε(ω). Further, the insignificant decrease of dielectric constant is observed with frequency increase up to 10^4kHz. Beginning from 10^4kHz the dielectric constant increases from 18,34 up to 20,64 for composition 10 vol.% $TlInSe_2$ and for composition 3vol.%Tl$\dot{I}nSe_2$, the dielectric constant increase from 18,8 up to 21,05 takes place in the same frequency interval.

In whole, the analogous change character ε(ω) is observed for composite 5 vol.% $TlInSe_2$, i.e. with frequency increase from 25 up to 100 kHz the dielectric constant increases from 22,87 up to 26,86. The dielectric constant decreases up to 23,56 with further frequency increase up to 10^4 kHz, with further frequency increase up to 10^6 kHz takes place the increase ε from 23,56 up to 26,68 for composites 10 vol.% and 3 vol.% $TlInSe_2$. However, in investigated frequency interval the dielectric constant of composite 5 vol.% $TlInSe_2$ is more than composites 10 vol.% and 3 vol.% Tl$\dot{I}nSe_2$. The frequency dependence of dielectric constant is firstly investigated in composites PE+ $TlInSe_2$ with aluminum nanoparticle, i.e. for composites

$$90vol.\%PE + 7vol.\%TlInSe_2 + 3vol.\%Al;$$
$$90vol.\%PE + 3vol.\%TlInSe_2 + 7vol.\%Al;$$
$$80vol.\%PE + 10vol.\%TlInSe_2 + 10vol.\%Al;$$
$$90vol.\%П0 + 5vol.\%TlInSe_2 + 5vol.\%Al;$$

In interval 25MHz-1 composites with aluminum nanoparticles are also obtained by above mentioned technology. As it is followed from fig.2b in whole investigated range takes place the insignificant decrease ε with frequency increase. The weakly-expressed maximum at frequency 200Hz is observed. The some exclusion is the composite 90vol%PE+5vol.%$TlInSe_2$+5vol.%Al for which takes place the ε increase in frequency interval 100kHz-1mHz.

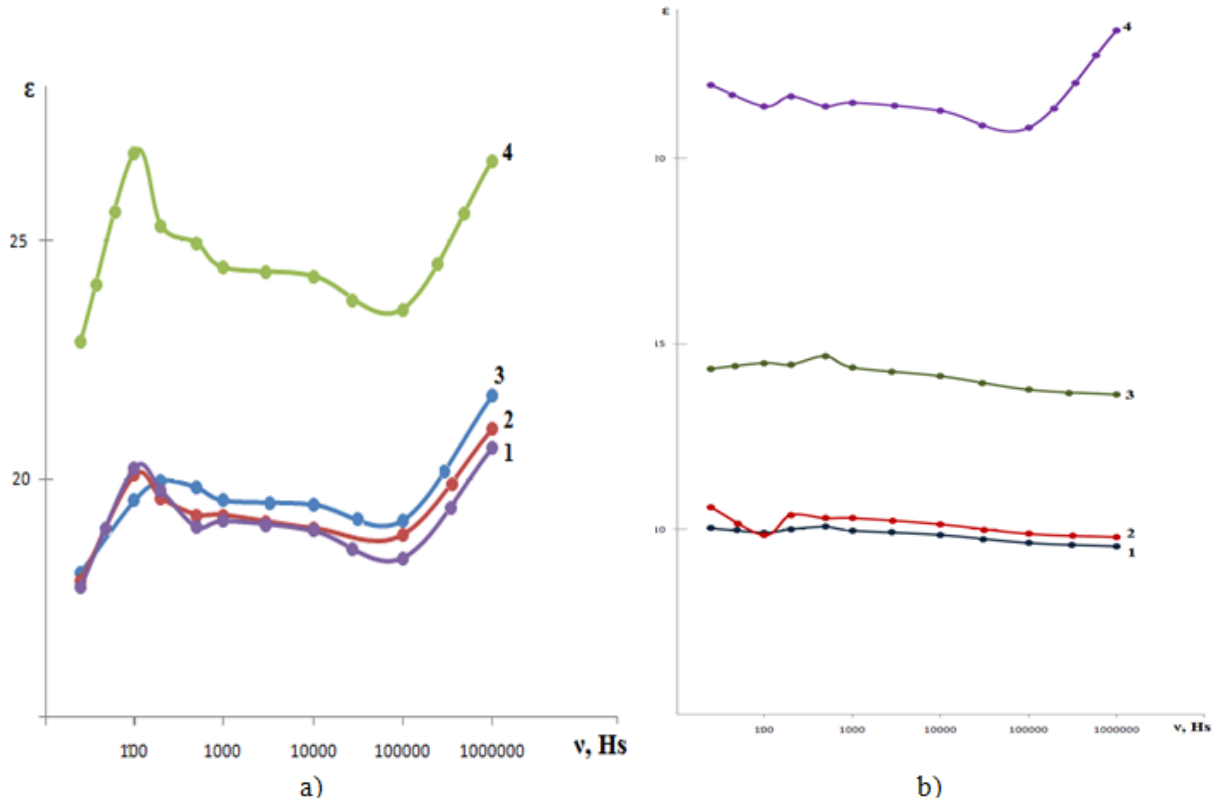

Fig. 2. The frequency dependence of dielectric constant of composites: a) $PE + xvol.\%TlInSe_2$ (1-x=10; 2-x=3; 3-x=1; 4-x=5), b) xvol.% PE+xvol.%$TlInSe_2$ + yvol.% Al (1-x=7, y= 3; 2-x=10, y=10; 3-x=3, y=7; 4-x=5, y=5)

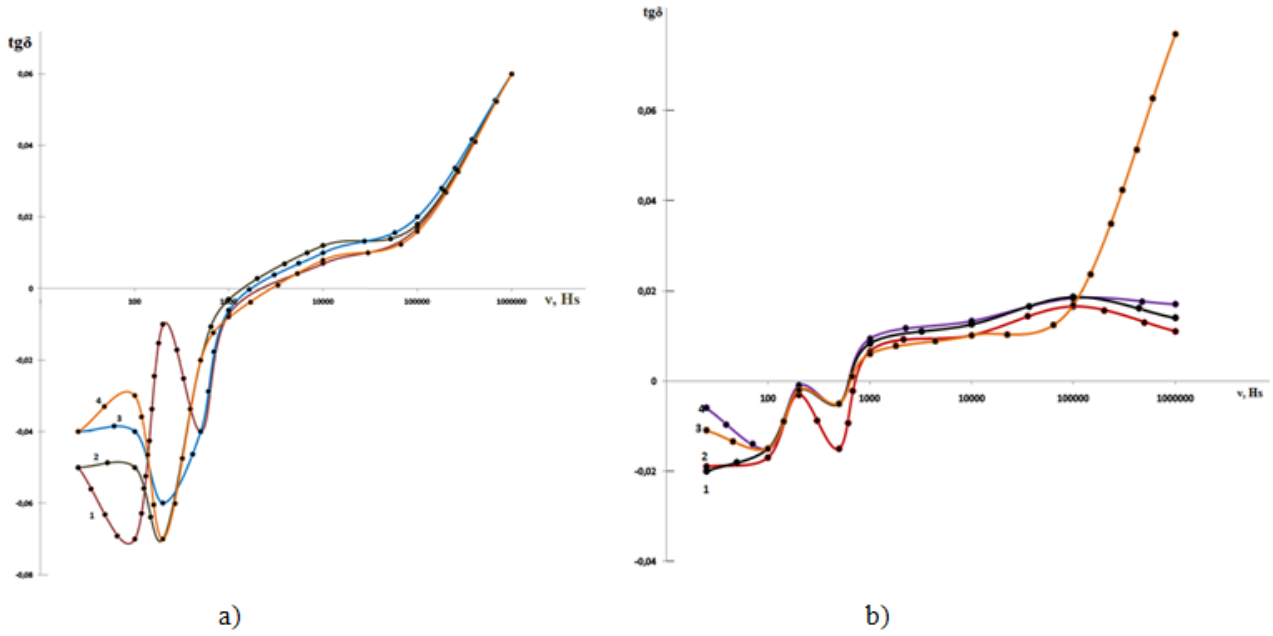

Fig.3. Frequency dependence of dielectric constant tgδ(ν) of composites: a) PE+xvol.% $TlInSe_2$ (1-x=1; 2-x=10; 3-x=5; 4-x=3) and b) PE + xvol.% $TlInSe_2$ + yvol.%Al (1-x=3, y=7; 2-x=7, y= 3; 3-x=5, y=5; 4-x=10, y=10).

In whole, with addition of aluminum nanoparticles into composite content, their dielectric constant stays practically constant in whole investigated frequency range, i.e. the dispersion in spectrum $\varepsilon(\omega)$ doesn't observed. The investigation results of dielectric losses of composites PE+ $TlInSe_2$ in dependence on frequency in range 25Hz-1MHz are given on fig.3 from which it is followed that for composite PE+1vol.% $TlInSe_2$ at 100Hz and 500Hz the deep maximums are observed, between them at frequency 200Hz the bright maximum is observed, after 500Hz firstly strongly increase and in frequency change from 1000Hz up to 100KHz the

moderate one are observed, further the strongly tgδ increase is observed. For composite PE+3vol.% $TlInSe_2$the maximum at frequency 100Hz is observed, the deep minimum at 200Hz, in range 200-1000Hz the maximum is strong one, in range from 1000Hz up to 100KHz is moderate tgδ increase and further the strong tgδ increase are observed. It is necessary to note that for composites with x=5; 10 the tgδ analogous changes are observed, i.e. for these composites the weak maximums are revealed at frequency 100Hz, deep minimum at 200Hz and further tgδ increase are observed.

The investigations are carried out on composites PE+ $TlInSe_2$ with aluminum nanopartcles. As it is followed from fig.3b for all investigated composites tgδ(ν) the dependence has similar character, i.e. at small frequencies for composites PE+5vol.% $TlInSe_2$+5vol.%Al, PE+10vol.% $TlInSe_2$+10vol.%Al the maximum decrease at frequency 200Hz is observed, the minimum at 500Hz, further increase up to 100KHz and insignificant decrease up to 1MHz are observed. For composites PE+3vol.% $TlInSe_2$+7vol.%Al; PE+7vol.% $TlInSe_2$+3vol.%Al at low frequencies (25-100Hz) the weak and further strong increase are observed, the maximum at 200Hz and deep minimum at frequency 500Hz are observed. It is necessary to note that tgδ change takes place analogously to other composites.

[1] *E.M. Godjayev, A.M. Magerramov, S.S. Osmanova, M.A. Nuriev, E.A. Allakhyarov*. Elektronnaya obrabotka materialov. 2007, 43(2), 84–88. (In Russsian)

[2] *E.M. Godjayev, A.M. Magerramov, S.I. Safarova, M.A. Nuriev, R.S. Ragimov*. Elektronnaya obrabotka materialov. 2008, 44(6), 66–71. (In Russsian)

[3] *A.M. Magerramov, S.I. Safarova, M.A. Nuriev, I.A. Safarova*. Elektronnaya obrabotka materialov. 2009, 45(2), 84–88. (In Russsian)

[4] *E.M. Godjayev, A.M. Maqerramov, Sh.A. Zeynalov, S.S. Osmanova, E.A. Allakhyarov*. Elektronnaya obrabotka materialov. 2010, 46(6), 91–96. (In Russsian)

[5] *Q.A. Mamedov, E.M. Godjayev, A.M. Magerramov, Sh.A. Zeynalov*. Elektronnaya obrabotka materialov. 2011, 47(6), 94-98. (In Russsian)

[6] *V.Yu. Petixov, M.I. Ibragimova, N.R. Xabibullina i dr*. Vliyanie strukturi polimernoy matritsi na ionnoluchevoy sintez tonkix metalopolimernix plenok. //Visokomolek. soed., ser.A, 2001, t.43, №11, s.1973-1983. (In Russsian)

[7] *S.S. Osmanova*. Avtoref. kand. dissert. Baku, BQU, 2007,s.23. (In Russsian)

[8] *A.V. Qoroxov, V.I. Zakrevskiy, I.M. Sokolova i dr*. Primenenie pezopolimerov v elektronnoy elektronnoy texnike // Plastiticheskie massi, 1988, № 6, s. 29-30. (In Russsian)

[9] *G.D. Guseynov, G.B. Abdullaev*. Pezorezistivnie effekti na monokistalax $TlInS_2$, DAN SSSR, 1973, t. 208, №5, s. 1052-1054. (In Russsian)

[10] *G.B. Abdullaev, G.D. Guseynov i dr*. Poluprovodnikoviy pereklyuchatel s pamyatyu A.s. №638194(SSSR). (In Russsian)

[11] *R.S. Ragimov, V.D. Rustamov*. Opticheskie pereklyuchateli na osnove monokristallov $TlInS_2$. XVIII Mejdunarodnaya nauchno-texnicheskaya konferenchiya po fotoelektronike i priborom nochnoqo videniya 25-28 maya 2004 g., Moskva, Rossiya. (In Russsian)

[12] *E.M. Qocayev, S.İ. Səfərova, R.S. Rəhimov, S.Ə. Zeynalov*. Elektret üçün kompozisiya materialı. Azərbaycan Respublikası Standartlaşdırma, Metrologiya və Potent üzrə Dövlət komitəsi. İxtiraya dair iddia sənədi barəsində məlumatın dərci haqqında qərar, №a20100033 tarix 28.12.2013. Potent (ixtira).

[13] *E.M. Godjayev, S.O. Guliyeva*. Azerbaydjan Texniki Universiteti, Elmi eserler №2, 2008. SCIENTIFIC WORKS. (In Russsian)

Received:07.11.2013

THE INFLUENCE OF UNCONTROLLED DEFECTS ON SINGLE CRYSTAL PHOTO-ELECTRIC PROPERTIES

F.I. MAMEDOV, G.S. MEHDIYEV, S.M. ZARBALIYEVA, E.K. GURBANOVA
Academy of emergency situations of Azerbaijan
Institute of Physics of Academy of Azerbaijan
AZ 1089, Baku, Azerbaijan,
AZ 1143, Baku, Azerbaijan.
famil.mammadov@fhn.gov.az

It is revealed that uncontrolled defects appearing at crystal obtaining and their treatment, strongly influences on $AgGaSe_2$, single crystal photo-electric properties obtained by Bridgman methods and electron processes taking part in forbidden band of single crystals, depend not only on light intensity and on sample perfection.

It is established that residual photo-conduction (RPhC) observation and its damping in $AgGaSe_2$ single crystals stimulated by light with different wave lengths are well explained on the base of known barrier model.

Keywords: damping of residual photo-conduction, uncontrolled defects.
PACS: 72.20.Dp, 72.20.-i, 81.10.Fq

INTRODUCTION

As it is known the semiconductor material properties are very sensitive to the smallest crystallization violations. The so-called uncontrolled defects are formed at semiconductor obtaining and sample treatment in crystal forbidden band that doesn't give the possibility to control the crystal growth process.

All these circumstances lead to the fact that crystals obtained and treated by different methods are different ones by their physical properties.

The last one makes difficult the understanding of the processes taking part in $AgGaSe_2$ single crystals especially at study of photo-electric properties.

In order to reveal the influence of such defects on photo-electric properties of investigated single crystals, the comparative investigations connected with some $AgGaSe_2$ photo-electric properties obtained at different technological conditions are carried out. The given article is dedicated to this problem.

The development of different storage units, storage elements of information accumulation on the base of semiconductors nowadays is the actual problem in connection with increasing requirements of computer engineering and automatics.

The optolectronic storage devices and photo-electric storage elements, i.e. devices which have the possibility of recording and storage of information given in the form of light signal, allows us to read information recorded on them by photo-electric or other type method many times without its elimination or distortion present the big interest. They are reversal ones, i.e. they allow us to delete the recorded information and to return in the initial state [1,2]. From this point of view the residual photo-conduction (RPhC) and its damping being the one of the most interest photoelectric effects in different semiconductor substances present the essential interest which includes in the fact that the high conductance saves in the sample during long period and it can be damped in necessary moment [3,4].

EXPERIMENTAL RESULTS AND THEIR DISCUSSION

The samples of $AgGaSe_2$ single crystals of two types obtained by chemical transport reaction and Bridgman-Stockbarger methods are used for investigation of photo-electric properties. In first case the samples aren't treated by additional mechanical treatment, in second case the polishing method is applied for obtaining of necessary forms and dimensions. The polishing is carried by following way: firstly the one side is polished by M30, M14 and M10 powders. Later, the sample is polished on cambric by diamond pasta by grain diameter in micron and polymicron. Further the other side is polished in the same sequence. After this the samples are polished up to necessary thickness. The samples are unsticked with the help of benzine and washed by alcohol. The average dimensions of the investigated crystals are $4\times1,6\times0,8$ mm^3 (obtained by chemical transport reaction) and $6\times4\times3$ mm^3 (obtained by Bridgman-Stockbarger method). The silver pasta, aquadaq and indium are used as contacts. For current measurements the same electric scheme is applied that in photo-conductions investigations. All measurements are carried out at 120K in metallic cryostat with vacuum by $\sim10^3$ mm Hg order at condition that sample supply voltage is in the limits of VACh linear region.

МДР-2, VSU-2 device is used in the capacity of monochromator. The incandescent lamp CH 8 serves the light source for stationary excitation. The light focuses on samples with the help of lens, the excitation intensity change is carried out by platinum attenuator and change of monochromator entrance slit width. The value of stationary photo-current is registered by recorder through amplifier.

The photocurrent relaxation curves in $AgGaSe_2$ single crystals taken after switching off and on the monochromatic light from proper absorption region at different values of incident light intensity are shown on fig.1.

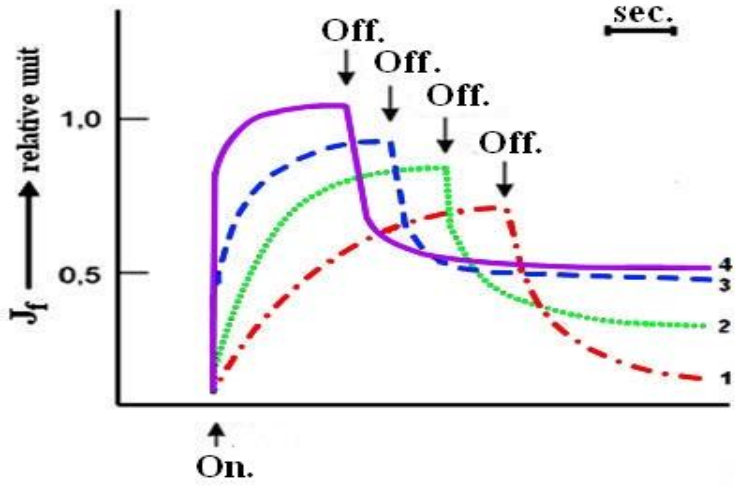

Fig.1. The relaxation curves of RPhC of $AgGaSe_2$ single crystals λ = 1,80eV.

The photocurrent relaxation curves in $AgGaSe_2$ single crystals taken after switching off and on the monochromatic light from proper absorption region at different values of incident light intensity are shown on fig.1.

The light intensity changes with monochromator entrance slit change. As it is seen the current slowly achieves its maximal value at low intensity after light switching on and decreases with time; the stationary photocurrent state is observed in some time. After light switching off the photoresponse decay takes place by law slower than simple exponential one and relaxes to different one from dark, new quasi-stationary value, i.e. RPhC in single crystals is observed. The image sensitivity increases with intensity increase and also growth velocity and photo-current decay correspondingly at light switching on and off. Thus, at small light intensity the establishment of stationary current value requires long time which decreases with intensity growth. As investigations show RPhC multiplicity (the relation of conductance in RPhC state to dark conduction) strongly depends on both the intensity and light wave length. As it is seen from the figure at small illumination dozes RPhC value linearly increases and at big dozes the saturation takes places. By other words at enough big duration and light intensity the RPhC multiplicity doesn't depend on intensity.

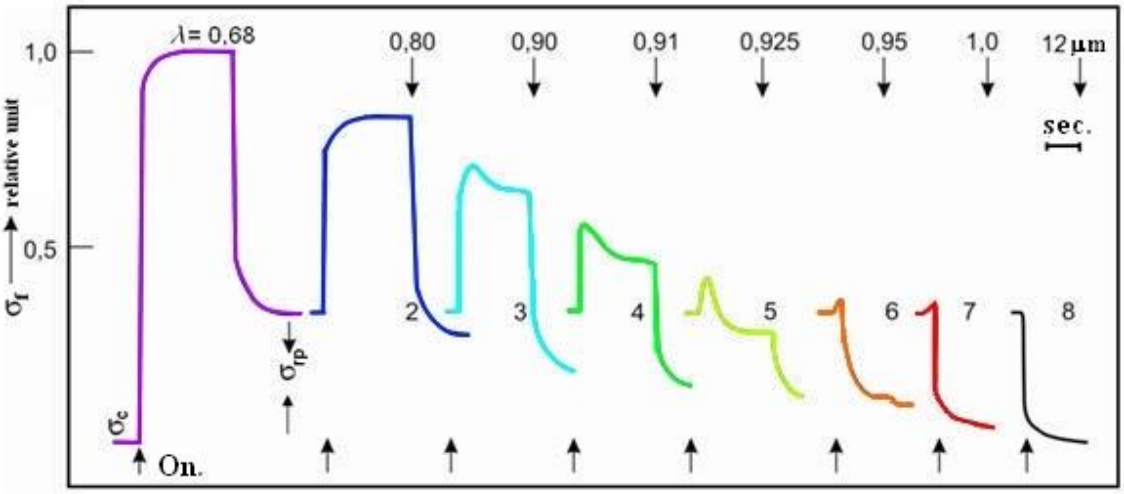

Fig.2. The damping kinetics of residual conduction at different wave lengths (T=120K).

The RC damping kinetics at different light wave lengths is presented on fig.2. These curves are obtained by following way. The sample is taken in cryostat and treated by illumination of proper light by wave length λ=0,68 mcm enough long time (20 minutes) at temperature 120K and further, it is endured in darkness up to achieving of stationary state (5 minutes). The RPhC level achieved by this is presented by σ_{res} region on figure. Later, the sample is illuminated by light with wave length λ=0,80 mcm. As a result the conduction strongly changes and when the photo-current achieves its stationary light value, the light is switched off and the cycle is repeated at other light wave lengths.

As it is seen from the figure, the curve character strongly depends on wave length of incident radiation. The light with wave lengths lying in region 0,80-0,95mcm leads to both photo-current increase and damping of residual conduction. For wave lengths more

than λ > 0,95a only RPhC damping is observed. It is necessary to note that the photo-current increase has "flare" character (curves 5-7) after light switching on of wave length λ=0,925 mcm and this "flare" character becomes the immediate one with increase of photon energy and finally, disappears at wavelength where only damping of residual conduction is observed.

In order to destroy the state with RPhC, it is enough to heat the crystal up to 400K and cool it in darkness. RPhC state and its damping can be repeated on the one and the same crystal many times.

It is necessary to note that the average value of multiplicity of proper RC is value ~10^2 and decreases with electric field increase and temperature increase. The RC observation only in $AgGaSe_2$ single crystals obtained by Bridgman-Stockbarger (RPhC in samples obtained by transport reaction is absent), its damping by IR-light and other experimental facts allow us to suppose that RC is connected with the presence of macroscopic potential barriers in the sample caused by semiconductor heterogeneity, consisting from regions of different resistance: low-resistance (LR) and high-resistance (HR) spacely separating the current carriers [2].

At this it is supposed that formed non-equilibrium carriers (electrons) accumulate in low-resistance region and create the additional conduction, holes are in high-resistance region and are captured by deep recombination centers after illumination of barrier region by proper light. The electron life time strongly increases because of introduction of slow recombination channel and the residual conduction is obtained.

IR damping of RPhC also can be explained on the barrier model language. The non-equilibrium carriers absorbed IR quantum save the energy enough for barrier overcoming and rapidly recombine with holes on centers in high-resistance region and RPhC damping is observed similar to IR damping, only here the residual conduction plays the role of phonon level.

The obtained experimental data show that RPhC spectrum in λ < 0,68 mcm region correlates with PhC spectrum and in wave length interval 0,68-1,5mcm RPhC damping is observed where usual positive impurity RC is observed in PhC spectrum. The RC damping region totally coincides with spectral dependence of IR damping of proper and negative PhC in investigated samples obtained by method of transport reaction. Such result gives us the foundation to propose that the potential barriers between high-resistance and low-resistance regions appeared in the samples obtained by Bridgman-Stockbarger (we propose that in our case the heterogeneity is connected with growing up or treatment of the crystal) are directly connected with the presence of τ-centers icreasing its sensitivity in both sample groups with similar energy from valence band top [5,6].

The damping effect only for wave lengths bigger than 0,68mcm is connected with the fact that quantum energy in this case is very small one, in order to cause the transitions leading to PhC increase and the curve form is defined by the ratio of velocities of excitation processes and PhC damping carrying out at the given light wave length .

Usually the excitation process takes place with big velocity causing the maximum appearance at switching on of additional illumination and minimum at its switching off.

The "flare" character of photocurrent at light switching on 1,0-0,90 mcm propably is caused by hole photo-ionization from centers [8]. As in $AgGaSe_2$ single crystals the levels are symmetrically situated relatively to forbidden band middle: $Evr = Ecr$ then crystal radiation by light with smaller energy $E<Evr$ into RC state causes simultaneous electron transitions from impurity level into conduction band and from valence band to impurity level. The positive current in the jump form is observed in the moment of impurity light switching on whereas excited electrons into C-band recombine with free holes through S-centers because of exhaust of capture levels and RC damping caused by the filling of $\tau -$ centers by electrons appears in some time. The recombination process velocity increases with the light wave length increase and photocurrent "flare" character correspondingly has the immediate character. The photocurrent "flare" character totally disappears and only the RPhC damping is observed (it is supposed that small levels E< 0,6 eV are totally filled by electrons and deep levels E>0,6 eV are filled by holes) when IR beams by wave lengths 0,6mcm excite the electrons from the valence band on slow τ – levels in high-resistance introductions and holes appearing at this, are "immediately" captured by S-levels where rapidly recombine with free photo-electrons. The supposed model also allows us to understand the fact that RPhC value practically doesn't depend on excitation level higher definite light intensity. Indeed, after ample illumination by weak light the filling of levels in low-resistance introductions up to some value corresponding to barrier height which defines the RPhC maximum value and consequently, the further intensity increases don't influence on RPhC value.

It can be proposed that RPhC damping mechanism by electric field and temperature increase is connected with overcoming of macroscopic potential barriers [9,10].

CONCLUSIONS

The residual conduction and its damping in $AgGaSe_2$ samples obtained by Bridgman method at 120K is firstly observed. It is shown how excitation and damping of residual conduction stimulated by the light with different wave lengths are explained on the base of known barrier model.

It is established that damping effect observation of only wave lengths bigger than 0,68 μм is connected with the fact that quantum energy in this case is extremely small one in order to cause the transitions leading to PhC increase.

It is established that RPhC value practically doesn't depend on excitation level higher the definite light intensity and damping mechanism by electric field and temperature increase is connected with overlapping of macroscopic potential barriers.

[1] *S.P. Gaplevskaya, L.S. Zavernitannaya, A.P. Rvachev.* Nekotorie osobennosti fotoelektricheskoy panyati CdS. UFJ 1974. T. 19. Vip. 2.s.292-295. (In Russian)

[2] *M.K. Sheynkman, A.Ya. Shik.* FTP 1976. T. 10. Vip. 2. s.209-233. (In Russian)

[3] *T.K. Kasumov.* Photocurrent ascultations Due to optimal phonons in $AgGaSe_2$ single crystals. Phys. Status Solidi A. 1989. № 2. p. 205-208

[4] *T.K. Kasumov. G.D. Guseynov, F.I. Mamedov.* Otrichatelnaya fotoprovodimost v monokrisstallax $AgGaSe_2$. Dokladi AN Azerb. SSR. 1988. T. 41. № 9. s.24-26. (In Russian)

[5] *A.Sh. Abdinov, A.G. Kyazim-zade.* FTP. 1976. № 12. s.2382-2385. (In Russian)

[6] *F.I. Mamedov, T.K. Kasumov.* Ostatochnaya providomost v monokristallax $AgGaSe_2$. Mater.Respub.konf.molodix uchenix ximikov. Baku. 1988. s.48. (In Russian)

[7] *F.I. Mamedov, S.F. Mextiyeva.* Petularitev of fotoelektreti property of single-cristals of $AgCaSe_2$. Progr. of Eurosiya conference on nuclear seans and i.v.s appilacation – october 2000 Turkey, s.437-438

[8] *S.G. Abdullaeva, A.V. Aliev.* Otrichatelnaya fotoprovodimost effekti *p* $TlInSe_2$. Dokladi AN Azerb. SSR. 1983. T. 39. № 3. s.23-25. (In Russian)

[9] *I.A. Karpovich, B.N. Zvonkov, M.I. Rizaxanov.* FTT.1970. T. 12. Vip. 8. s.855-858. (In Russian)

[10] *F.I. Mamedov.* Azərbaycan Mühəndislik Akademiyasının Xəbərləri, № 4, 2012, c. 13-19. (In Russian)

Received:04.11.2013

THERMAL EXPANSION AND ISOTHERMAL COMPRESSIBILITY OF $InGaTe_2$ COMPOUND

E.M. GODJAYEV, U.S. ABDURAKHMANOVA
Azerbaijan Technical University G.Javid str., 25, Baku
geldar-04@mail.ru

The investigation results of temperature dependences of thermal expansion coefficients and isothermal compressibility of $InGaTe_2$ triple compound crystallizing in tetragonal syngony with space symmetry group D_{4h}^{18} having the parameters of elementary cell *a*=8,463Å; *c*=6,981Å and chain structure are given in the given work. It is revealed that in investigated temperature interval 80-350K the anomalies in dependencies $\delta(T)$ and $\chi_T(T)$ aren't observed.

Keyword : isothermal compressibility ,band structure, vibrational contour
PACS: 43.35.Bf; 61.20.Gy; 82.60.Lf

INTRODUCTION

The existence of triple compounds $A^{III}B^{III}X_2^{VI}$ are already informed in works [1,2]. By decryption of crystal structure TlSe it is revealed that in the content of the given phase the thallium atoms have the alternative valence, i.e. the half of thallium atoms have the univalence and other part of atoms have the trivalence and chemical formulae TlSe can be written in the following form:

$$TlSe \rightarrow Tl^{+}Tl^{3+}Se_2.$$

Further, with exchange of trivalent TlSe by trivalent elements of third group the new class of semiconductor compounds of type $A^{III}B^{III}X_2^{VI}$ are obtained and investigated. $InGaTe_2$ is structural analogue of the compounds of above mentioned types crystallizing in tetragonal syngony with chain structure. At $InGaTe_2$ formation the external electron configurations of two tellurium atoms $2(5s^2 5p^4)$, because of one $5p^1$ indium electron and three $4s^2 4p^1$ gallium ones are constructed up to neutral configuration $2(5s^2 5p^6)$.

The elementary cell $InGaTe_2$ has the two formula units. In crystal lattice $InGaTe_2$ the univalent In atoms are surrounded by eight Te atoms whereas trivalent Ga atoms are in tetrahedral surrounding of Te atoms and form the atom chains $(Ga_3^{+}Te_2^{-2})^{-}$ prolonged along optical axis *c*. Nowadays the some properties and electron spectrum [3-5].

The band structure calculation of the given phase shows that valence band $InGaTe_2$ consists of three subbands. The low subband consisting of four bands is far from rest ones by wide energy gap by order – 6eV. The theoretic-group analysis shows that these low valence bands are situated near $-10 \div -11$eV are bind to *5s*-states of Te.

The following group from four valence bands situated on energy level near -5eV is originated from mainly s-states of In and Ga atoms. The rest big group from ten bands by 5 eV thicknesses is originated from p-states of In, Ga and Te atoms.

The aim of the given work is the investigation of temperature dependence of thermal expansion coefficient (TEC) and isothermal compressibility (IC) $InGaTe_2$**.**

EXPERIMENTAL PART

For investigation of thermal expansion coefficient and isothermal compressibility $InGaTe_2$ the samples are obtained by following way. At synthesis $InGaTe_2$ the elements by pureness In-000, Ga-99, 996, Te-0.067% are used. The ampoules firstly are refined by mixture HF of distillated water. After chemical refining the ampoule evacuated up to 0, 0133 Pa are put into stove at 1000^0C on 24 h after it is cooled, filled by high-purity elements. For melt homogenization the mixture is endured 24 hours at temperature 970^0C. During synthesis process the ampoules are often shaken out with the aim of best mixture of component parts. Further, the ampoule with substance with rate 1,33mm per hour is transferred from high-temperature band into crystallization one with corresponding temperature 700^0C. After cooling up to room temperature the obtained crystals are treated by X-ray analysis. It is revealed that compound $InGaTe_2$ crystallizes in tetragonal syngony is monophase one with lattice parameters $a = 8{,}463(7)$ Å $c = 6{,}981(8)$ Å These values are well agree with data [5] where $a = 8{,}412$ Å, $c = 6{,}875$ Å.

For measurement of temperature dependencies of thermal expansion coefficient and isothermal compressibility $InGaTe_2$ the installation is used by us, described in work [6]. The principal scheme of extension registration developed in work [6] consisting of generator oscillating loop and high-frequency amplifier on one transistor has some disadvantages. In particular, there is no reliable agreement between scheme output and outputs of numerical measuring devices and negative influence of sinusoidal oscillations on the work of numerical frequency meters.

That's why for elimination of these disadvantages the additional transformer of sinusoidal oscillations into numerical one is introduced into scheme. It consists of three elements «and - not». The first element of micro-scheme is carried out as threshold one and amplifier the output of which is numerical one. Further, the signal passes through two elements «и - не» and finally formed it comes on input of numerical frequency meter. In system of extension registration (fig.1) all capacitor are mica ones (excluding paper one C^1), transistor T^1 – КТ361В and also stabilitron КС447А, micro-scheme К555ЛА3 with

any other blade letters. The resistors of МЛТ- 0,25 type. The supply voltage is 14V. The oscillations frequencies are measured by frequency meters of Ч3- 33 type.

The measurements on installation are carried out in following consequence: for heating on investigated sample which can have any geometric form (the samples of cylindrical form with diameter 5mm and length 30mm) along whole length round to round the constant wire by diameter 0,1mm with silk isolation is bifilar rounded. Further, its surface is covered by thin layer of glue БФ-2 that is promoted to slow and uniform temperature change of all sample parts. The sample temperature is measured at 77,3-400K by cuprum-constant thermo-couple. For measurement reliability we take three pairs of thermo-couples which are glued to upper, middle and lower sample parts.

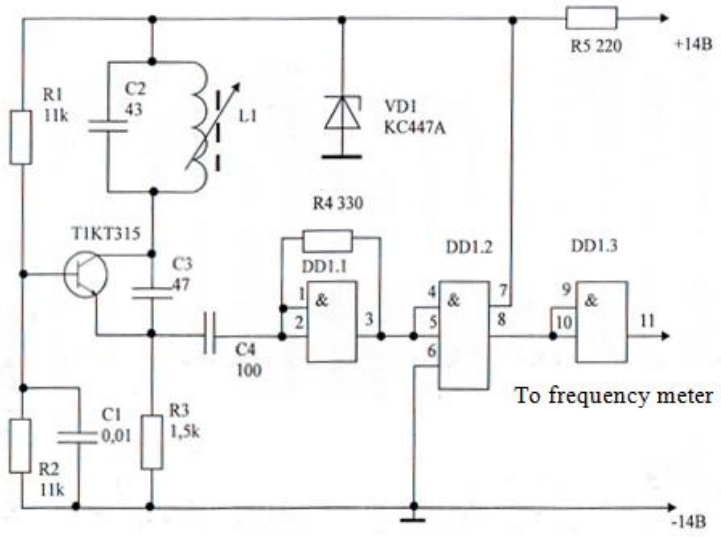

Fig.1. Principal scheme of registration system of sample change.

RESULTS AND THEIR DISCUSSION

KTP $InGaTe_2$ investigation is carried out in temperature interval 80-350K. the results are given on fig.2a. As it is followed from fig.2a with temperature increase from 80 up to 230K KTP increases and from further temperature increase stays practically constant. The insignificant structure is observed at temperature 198K on dependence $\delta(T)$. The other anomalies in $\delta(T)$ dependence aren't observed.

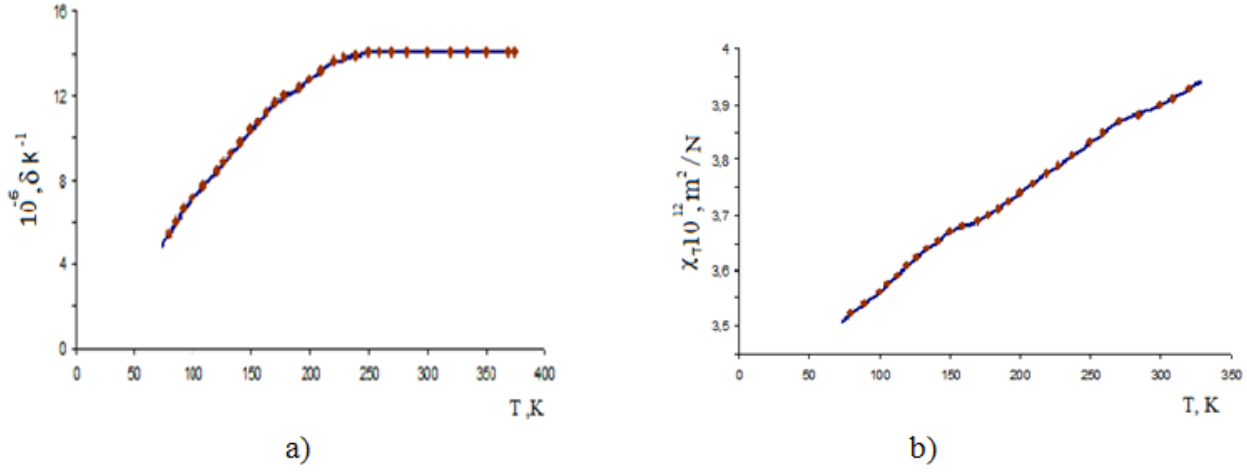

Fig.2. Temperature dependencies of thermal expansion coefficients (a) and isothermal compressibility (b) $InGaTe_2$.

The investigation results of IC $InGaTe_2$coefficient are given on fig.2b. As it is seen, IC increases with the temperature increase from 80 up to 350K. The insignificant structure is observed on curve $\chi_T(T)$ at temperature 198K. The other anomalies aren't observed on $\chi_T(T)$ dependence.

The analysis of obtained results shows that at low temperatures in difference from Grunayzen law KTP strongly increases. Such dependence is revealed for other crystals [7]. So for explanation of inclinations from Grunayzen law at low temperatures the study of physicochemical crystal properties is paid more attention. Thus, for obtained results the Grunayzen known

expressions are necessary improved. KTP connection with other thermodynamical values can be defined taking under consideration the dependence of Grunayzen coefficient on temperature

$$\delta = \gamma \frac{C_V \gamma_T}{V} + \left(\frac{\partial \gamma}{\partial T}\right)_V \frac{E \chi_T}{V},$$

here E is internal energy, V is molar volume, C_V is thermal capacity at constant volume, χ_T is isothermal compressibility coefficient. From the given expression as the private case $\left(\frac{\partial \gamma}{\partial T}\right)_V = 0$ Grunayzen formulae is obtained. Grunayzen constant plays the essential role at construction of theory of solid bodies and bonds the thermodynamic parameters [8]. As it is followed from formulae γ characterizes the unharmonicity of interacting forces, because other values in right side of expression are obtained from harmonic approximations. This formulae can be used by someone when the γ = const expression can be accepted. As it is above mentioned, the chemical formulae $InGaTe_2$ can be written in the form $In^{+}(Ga^{+3}Te_2)$ then In and Ga atoms take two different crystallographic positions. In compounds of this type between ions the relatively weak chemical bond is observed. Probably, KTP increase including IC takes place in the direction of chain between In^{+} Te_2 ions.

[1] *H. Hahn, B. Weltman.* Üder ternare chalkogenide des Thalliums mit Gallium und Indium. Naturwissenschaften, 1967, v. 54, No. 2, pp.42.

[2] *M. Müller, G. Eulenberger und H. Hahn.* Über ternare Thalliumchalkogenide mit thalliums-selennid-structur. Z. anorg. allg. chem.1973, v. 398, No. 2, pp. 207-220.

[3] *E.M. Gojayev, P.F. Aliyeva, R.S. Ragimov, U.S. Abdurakhmanova, A.A. Ismailov.* Raschet zonnoy strukturi i opticheskikh funktsiy troynikh soedineniy $InGaSe_2$, $InGaTe_2$. Materiali VIII Mejdunarodnogo simpoziuma «Fundamentalnie i prikladnie problemi nauki», Moskva, I tom , 2013, s.59-67.

[4] *U.S. Abdurakhmanova.* Zone structure of $InGaTe_2$ compound. I International Scientific Conference of Young Researchers,Proceedings, s.278-279.

[5] *M. Mobarak, H. Berger G.F. Lorusso, Y. Capozzi, G. Pernaмo, M. Ibrahinl, G. Margaritondo*.The growth and properties of single crystals of I_{nGaTe_2}, ternary chalcogenide semiconductor r/J.P hys.D: Appl. Phys., 1998,3 1, p. 1433-1437.

[6] *E.M. Gojayev, M.M. Zarbaliyev, M.M. Kurbanov*. Dilatometr dlya izmereniya TKLR tverdikh tel v shirokom intervale temperatur. Izmeritelnaya tekhnika. 1985, n.2, s. 44-45.

[7] *S.I. Novikova.* Sb. «Fizika tverdogo tela i termodinamika», Novosibirsk, 1972, s.56.

[8] *S.I. Novikova*. Teplovoe rasshirenie tverdikh tel. Moskva: Nauka, 1974, s.278.

Received:05.11.2011

SYNTHESIS OF CdS AND ZnS NANOCRYSTALS IN THE TEMPLATE OF MALEIC ANHYDRIDE-OCTENE 1-VINYL BUTYL ETHER TERPOLYMER

E.Y. MALIKOV, O.H. AKPEROV, M.B. MURADOV, G.M. EYVAZOVA
Baku State University, Z.Khalilov str.,23, Baku, Azerbaijan AZ – 1148
E-mail: bsuc@hotmail.com

Maleic Anhydride–Octene-1–Vinylbutyl Ether terpolymer has been synthesized via the radical terpolymerization method in order to prepare a new matrix for synthesis of CdS and ZnS nanocrystals. CdS and ZnS nanocrystals were separately synthesized in N,N–dimethylformamide solution of terpolymer through the reaction of thiourea with cadmium chloride and zinc chloride. Synthesized nanocomposites were characterized using several methods like Energy dispersive X–ray analysis and Transmission Electron Microscopy to obtain the proof results of nanocrystal formation. According to the results obtained with Transmission Electron Microscopy investigation the sizes of these nanoparticles do not exceed 5 nm.

Keywords: Terpolymer; nanocrystals; transmission electron microscopy (TEM); Energy Dispersive X–ray analysis (EDX)
PACS: 82.35.Np

1. INTRODUCTION

Nanotechnology deals with materials or structures in nanometer scales, typically ranging from subnanometers to several hundred nanometers. One nanometer is 10^{-3} micrometer or 10^{-9} meter. Nanotechnology is a new field or a new scientific domain. On nanometer scale, materials or structures may possess new physical properties or exhibit new physical phenomena. Nanomaterials attract many scientists and engineers due to their unique electronic, mechanical, thermal, chemical properties associated with their size. There may be many more unique physical properties not known to us yet. These new physical properties or phenomena will not only satisfy everlasting human curiosity, but also promise new advancement in technology [1].

Nowadays sulphide semiconductors with nanometer size dimensions have been the focus of many researchers due to their specific properties. Therefore CdS nanocrystals are very interesting for several researchers because of their variety of applications such as photonic materials. CdS nanocrystals are well-studied semiconductors because of their stability, easy preparation and distinct band gap that helps to detect a number of optical phenomena [2,3].

Many useful methods have been used for preparing II–VI group sulphide semiconductor nanoparticles, such as colloidal chemistry method, sol – gel method, inverse micelle method, in situ synthesis and assemble on polymer template.

The most significant method is in situ synthesis and assembly of sulphide semiconductor nanocrystals on polymer. It is realized by loading metal ions uniformly on polymer and then reacting metal ions with S^{2-} ions to form sulphide nanoparticles [4].

In this paper Maleic anhydride–Octene 1–Vinylbutyl Ether terpolymer (TPL) has been used as template for synthesis of CdS and ZnS nanoparticles. Novelty of this work is the first time use of the TPL as the matrix for synthesis of CdS and ZnS nanocrystals.

The goals of the present work are following: a) obtaining new matrices for synthesis of CdS and ZnS nanocrystals; b) synthesis of CdS and ZnS nanocrystals in TPL matrix and the prove of the formation of nanocrystals in the TPL. The advantage of the obtained material is the use of this material in solar cell and semiconductor fabrication.

2. EXPERIMENTAL

2.1. Materials and methods

All the chemicals were of analytical reagent grades. Maleic anhydride (MA) was purified before use by recrystallization from benzene and by sublimation under vacuum. Octene-1 (OC), Vinylbutyl ether (VB), and butyl acetate (BA) were distilled before use. Azobisisobutyronitrile (AIBN) was purified by recrystallization from ethanol.

Energy Dispersive X-ray analysis (EDX) have been carried out with EDX RÖNTEC Quantax analytical device.

Transmission Electron Microscopy images have been taken with FEI TECNAİ G2 20 X-TWIN Transmission Electron Microscope using 200 kV voltage. The TEM specimens were prepared by dripping the droplets of the N,N-dimethylformamide solution of terpolymer / CdS and terpolymer / ZnS nanocomposite onto the carbon coated copper grid.

2.2. Preparation of Maleic anhydride-Octene-1-Vinylbutyl ether terpolymer (TPL)

First of all TPL was synthesized. Synthesis process was free radical terpolymerization method. The process was performed in butyl acetate solution in the presence of AIBN as an initiator.

9.8 g of MA (0.1mole), 4.85 ml of VB (0.05 mole), 5.85 ml of OC (0.05 mole), and 0.2 g of AIBN was thoroughly dissolved in 50 ml of butyl acetate and poured into ampule.

Then this ampule was immersed into glycerine bath and temperature was raised to 80°C. Heating was continued for 4 hours. Thermostat was used for stabilization of the temperature. After 4 hours TPL was precipitated from solution with isopropyl alcohol, washed several times, and dried in vacuum.

2.3. Synthesis of CdS and ZnS nanocrystals in previously formed TPL template

Apparatus for CdS and ZnS nanocrystal synthesis in previously synthesized TPL was assembled using following parts:

Three-necked round bottom flask (500 ml), reflux condenser, water bath, stirrer, thermometer, heater, stand and clamps. 1.0 g of TPL was dissolved in 100 ml of N,N-dimethylformamide (DMF) to form a polymer solution at room temperature. Then 0.48 g of $CdCl_2$ x 2.5 H_2O (2.1 x 10^{-3} mole) was added to the polymer solution and this solution was stirred vigorously in a three necked round bottom flask. The temperature was raised slowly to 90°C and the mixing was continued for 4 hours. After 4 hours 0.76 g of thiourea (0.01 mole) in DMF was then injected into the reaction flask using a syringe with vigorous stirring. The reaction was continued for another 1 hour, and a yellow clear solution was obtained which indicated the formation of CdS nanocrystals. The same process was performed for ZnS nanocrystal synthesis, too.

3. RESULTS AND DISCUSSION

3.1. Energy dispersive X–ray (EDX) analysis

EDX is an analytical technique used for the elemental analysis or chemical characterization of a sample. It relies on the investigation of an interaction of some source of X – ray excitation and a sample [5].

This method has been used for elemental structure characterization of TPL / CdS and TPL / ZnS nanocomposite. It can be seen in the EDX spectrum for TPL / CdS that there are carbon, nitrogen, oxygen, sulfur, chlorine, and cadmium in the sample (figure 1). Spectrum of TPL / ZnS (figure 2) shows results for carbon, nitrogen, oxygen, sulfur, chlorine, and zinc. Carbon and oxygen are the elements from terpolymer matrix. Nitrogen is not expected element in this case. The origin of nitrogen participation in the sample is AIBN. That is an initiator. When it decomposes it gives the radicals with cyanide groups which contain nitrogen in it. These radicals begin the radical polymerization process and remain in the macromolecule.

Peaks of cadmium, zinc and sulfur are the evidences of CdS and ZnS formation in the matrix.

$CdCl_2$ x 2.5 H_2O and $ZnCl_2$ x 2.5 H_2O were used as the precursors in this process. Some parts of the precursors may remain unreacted in the system and that is the reason of observation of the peak of chlorine in the spectrum.

3.2. Microscopic characterization

Transmission Electron Microscopy is the most useful microscopy method in nanotechnology. This is a microscopy technique whereby a beam of electrons is transmitted through an ultra thin specimen, interacting with the specimen as it passes through. An image is formed from the interaction of the electrons transmitted through the specimen.

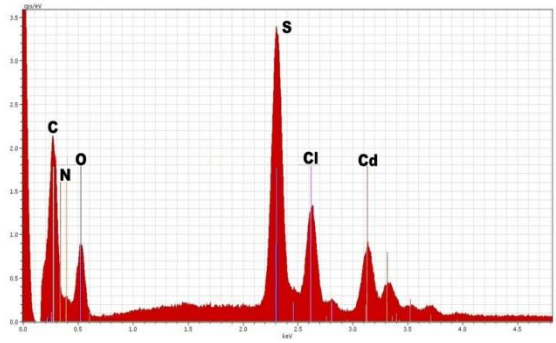

Fig. 1. Energy Dispersive X-ray spectrum of TPL / CdS nanocomposite.

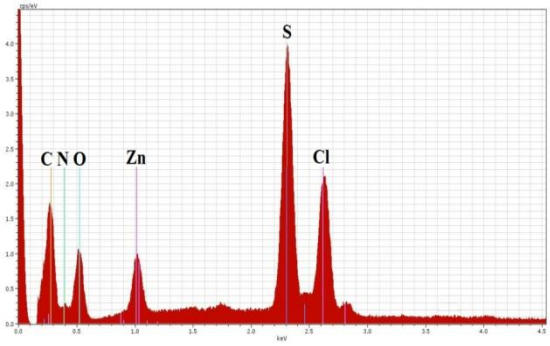

Fig. 2. Energy Dispersive X- ray spectrum of TPL / ZnS nanocomposite.

The presence of nanoparticles in polymer matrix can be easily proven with Transmission Electron Microscope.

Figure 3 and figure 4 show TEM images of CdS and ZnS nanocrystals. These images are in 50 nm scales and they are the evidences of participation of CdS and ZnS nanoparticles in polymeric matrix. It can be deduced from the images that the sizes of the synthesized nanocrystals do not exceed 5 nm and that is expected size. It is obvious that the physicochemical properties of the nanoparticles improve with decreasing of the size. And the obtained sizes are quite good to get unique properties.

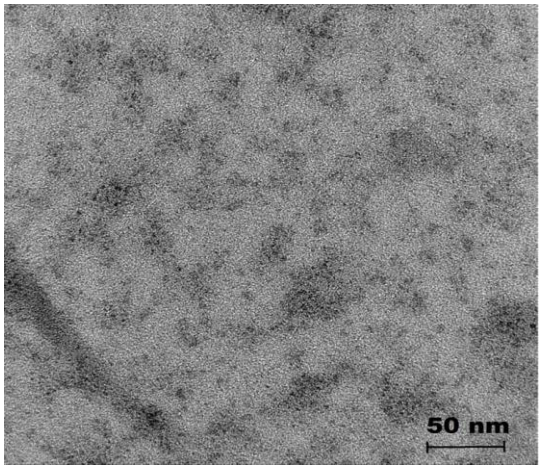

Fig. 3. TEM image of the CdS nanocrystals.

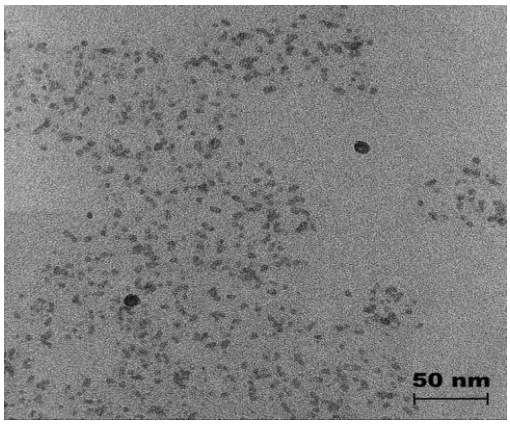

Fig. 4. TEM image of the ZnS nanocrystals.

4. CONCLUSIONS

In the present work TPL was synthesized via radical terpolymerization method. Then this terpolymer was used as the matrix in CdS and ZnS nanocrystal synthesis process. CdS and ZnS nanocrystals were synthesized through the reaction of cadmium chloride and zinc chloride with thiourea.

EDX results show that synthesized sample consists of carbon, nitrogen, oxygen, sulfur, chlorine, cadmium and zinc.

TEM images of the obtained nanoparticles show that the sizes of these nanoparticles do not exceed 5 nm. This is an expected size for nanocrystals obtained with this method.

According to obtained results it is easy to say that, the synthesis method used in this paper is useful for nanoparticle synthesis purpose and can be used as the industrial method in the future.

ACKNOWLEDGMENT

This work was supported by the Science Development Foundation under the President of the Republic of Azerbaijan–Grant № EIF–2012–2(6)–39/26/4. Some parts of the work were performed under support of EC FP7 NAPEP (Grant agreement number: 266600) grant and the Baku State University 50+50 grant.

[1] *Guozhong Cao*. Imperial College Press, (2004).
[2] *S. Gorer, G. Hodes*. J. Phys. Chem., 98, 5338 (1994).
[3] *I. Chakraborty, D. Mitra, S.P. Moulik*. J. Nanopart. Res., 7, 227 (2005).
[4] *L.D. Sun, B. Xu, X.F. Fu, M.W. Wang, C. Qian, C.S. Lian, C.H. Yan*. Sci. China.: Series B, 44(1), 23 (2001).
[5] *J. Goldstein*. Scanning Electron Microscopy and X - Ray Microanalysis, Springer, (2012).

Received:07.11.2013

OPTICAL FUNCTIONS OF $InGaSe_2$

E.M. GODJAYEV[1], P.Ph. ALIYEVA[2], M.H. ALIYEVA[3], I.A. SAFAROV[3]
Azerbaijan Technic University[1]
Baku, G. Javid str., 25
Salyan department of Institute of Teachers of Azerbaijan[2]
Azerbaijan State Oil Academy[3]
G.Javid str., 25, Baku
geldar-04@mail.ru

The calculation results of optical functions: imaginary and real parts of dielectric constant, main index of refraction and its imaginary part , reflection coefficient and imaginary part of reverse value of complex dielectric constant, real and imaginary parts of optical electric conduction of $InGaSe_2$ compounds at **e**||**c** and **e**⊥**c** polarizations in energy intervals 0-12eV, are given in the work.

Keywords: optical electric conduction, spectral functions, complex dielectric constant
PACS: 72.40.+w, 73.50.Pz **...**

The semiconductor compound $InGaSe_2$ is related to tetragonal syngony of D_{4h}^{18} group, elementary cell has two formula units, lattice constants a=8.0511 Å, c=6.3174 Å, chalcogenide parameters x=0.1636. In crystal lattice $InGaSe_2$ the univalent atoms are surrounded by eight Se atoms, whereas trivalent Ga atoms are in tetrahedral surrounding of Se atoms and form the atom chains ($Ga_3^+Se_2^{-2}$) prolonged along optical $\vec{c}$ axis.

In scientific literature there are information about structure investigation and properties of triple compound $InGaSe_2$ [1-5]. However, there is no information about investigation of $InGaSe_2$ optical properties. In this connection in the given work the calculation results of optical functions of given phase are given.

The optical functions $InGaSe_2$ are calculated by known technique given in [6]. At obtaining of spectral dependence of imaginary part of complex dielectric constant we use the relation:

$$\varepsilon_i(E)=\frac{N}{E^2}\sum_{k\in BZ}\sum_{v,c}\left|\mathbf{e}\cdot\mathbf{M}_{cv}(\mathbf{k})\right|^2\delta\left(E_c(\mathbf{k})-E_v(\mathbf{k})-E\right), \tag{1}$$

where

$$\mathbf{e}\cdot\mathbf{M}_{cv}(\mathbf{k})=\mathbf{e}\cdot\int\psi_{ck}^*(\mathbf{r})(-i\hbar\nabla)\psi_{vk}(\mathbf{r})d^3r\cdot$$

This integral is taken over the volume of crystal elementary cell and means the matrix element of impulse operator $\mathbf{p}=-i\hbar\nabla$; v and c indexes number the states of valence band and conduction band, correspondingly; **e** is unit factor of polarization. At summation over Brillouin zone in (1) the elementary cell of reverse lattice is divided on 64 equal volume parts and in them occasionally **k**-points are chosen. About 3000 points are taken, as a result of which the histogram is obtained. N constant is defined from the condition of histogram normalization $\int_0^\infty E\varepsilon_i(E)dE=\frac{\pi}{2\hbar^2}\omega_p^2=\frac{\pi}{2\hbar^2}\cdot\frac{4\pi n_e e^2}{m_e}$, where ω_p is plasma frequency for electrons; n_e is average electron density in crystal.

The histogram is constructed with the step 0,2eV and covers all interband transition $v\rightarrow c$ with energy up to 12eV. Beginning with small structure in histogram near 12eV the $\varepsilon_i(E)$ dependence is extrapolated by known formulae $\varepsilon_i(E)\big|_{E\rightarrow\infty}\sim E^{-3}$. The transitions from lowest bands having Se-5s origin are partially into investigated spectral region. These bands are situated far away and as our investigations show the widening of spectral region and introduction of big energy transitions from these bands in high states of conducting bands doesn't lead to contributions in dielectric constant significantly differing from extrapolation.

The real part of dielectric constant is defined from integral dispersion relation of Kramers-Kroning:

$$\varepsilon_r(E)=1+\frac{2}{\pi}P\int_0^\infty\frac{E'\varepsilon_i(E')\cdot dE'}{E'^2-E^2}\quad . \tag{2}$$

Here the integral is designated by P symbol in meaning of the main value.

The calculation results of above mentioned spectral functions of $InGaSe_2$ compound for **e**||**c** and **e**⊥**c** polarization are given on fig.1a and 1b. As it is seen from fig.1a in interval 1.85 – 3.05eV the calculative curves rapidly increase up to maximum. According to these figures the maximum of the main peak in $\varepsilon_r(E)$ spectrum at **e**||**c** (fig. 1a) polarization is at energy 2.55eV and at **e**⊥**c** (fig. 1b) 2.75 eV in $\varepsilon_i(E)$ spectrum in both polarizations the maximums of the main band which we connect with transitions from upper part of valence band into lower conducting bands are at 3.5eV. In $\varepsilon_i(E)$ spectrum at **e**⊥**c** polarization there are four peaks with energies 4.25, 5.55, 5.95 and 6.45eV. At **e**||**c** polarization the additional peaks are situated at energies 4.05, 5.08 and 5.75eV, but they are weakly expressed, mainly the last ones.

The maximum value ε_i at polarization **e**||**c** is equal 24.9 and at 14.95; such difference is character for chain crystals by $InGaSe_2$ type with strong anisotropy. The limit value $\varepsilon_r(E=0)$ is equal to 9.5 at polarization **e**||**c** and 9.1 at **e**⊥**c**.

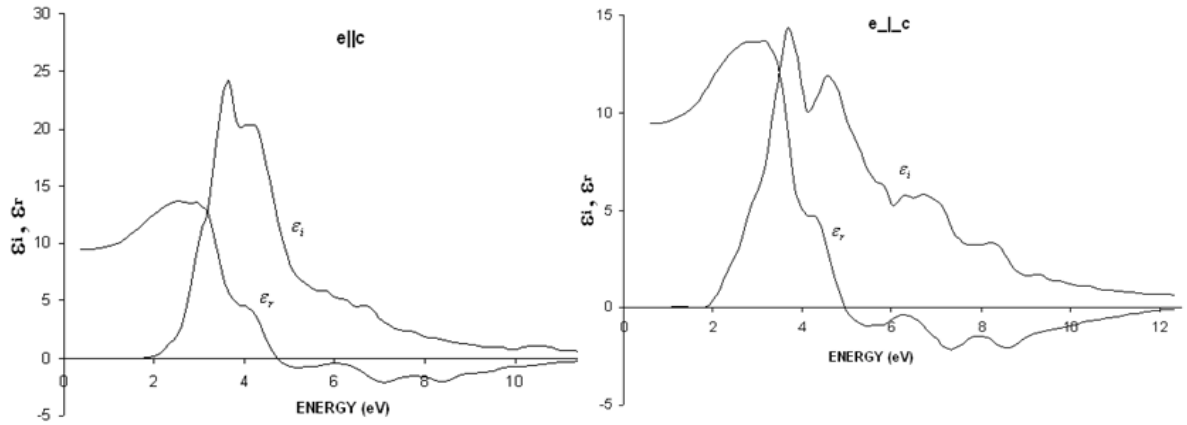

a) b)

Fig.1. The spectral dependence of (ε_i) imaginary and (ε_r) real parts of dielectric constant of $InGaSe_2$ compound for **e**||**c** (a) and for **e**⊥**c** (b) polarization.

The optical functions of the given phase are calculated with the use of value of real and imaginary parts of dielectric constants of $InGaSe_2$. The main refraction index (refraction real component) is defined by the formulae:

$$n = \sqrt{\frac{1}{2}\left(\varepsilon_r + \sqrt{\varepsilon_r^2 + \varepsilon_i^2}\right)},$$

The energy dependence of the main refraction index is given on fig.2a. As it is followed from fig.2a at **e**||**c** polarization the ***n****(E)* dependence has the maximum at energy 3.2eV (***n***=3.87) up to energy 12eV.

The clear expressed maximum (***n***=3.92) and further decrease ***n*** is observed on ***n****(E)* spectrum at **e**⊥**c** polarization. For the givven polarization at energy 8.65eV (***n***=0.71) is revealed the insignificant structure.

The spectral dependence of the imaginaty part of refraction index of $InGaSe_2$ compound at **e**||**c** and **e**⊥**c** polarizations is carried out on fig.2b. As it is followed from fig.2b at **e**||**c** polarization the clear expressed maximum and in further energy **k** decreases from 2.99 up to 0.99 is revealed on **k** *(E)* spectrum. In case of **e**⊥**c** polarization the maximum revealed at **e**||**c** polarization makes double. The first maximum is revealed at 3.68eV, the second maximum is revealed at 4.58eV. Between these maximums at 4eV the clear expressed minimum is revealed. Beginning from energy 4.58eV, **k** decreases up to energy 8.65eV and after it strongly increases.

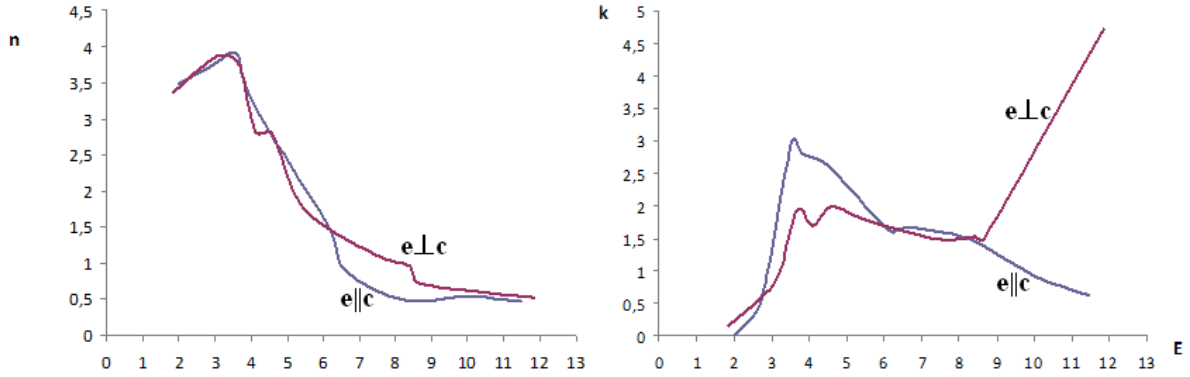

a) b)

Fig.2. Energy dependence of refraction main index ***n****(E)* (**a**) and imaginary part of refraction coefficient **k** *(E)* (**b**) of $InGaSe_2$ compound for **e**||**c** and for **e**⊥**c** polarization.

The reflection coefficient at normal light falling is defined by formulae:

$$R = \frac{(n-1)^2 + k^2}{(n+1)^2 + k^2},$$

The spectral dependence of reflection coefficient of $InGaSe_2$ compound for **e**||**c** and **e**⊥**c** polarizations is given on fig.3a. As it is seen from fig.3a ***R****(E)* spectrums at **e**||**c** polarization the two maximums at 3.54eV and 8.27eV energies correspondingly and minimum at energy 6.09eV appear. After second maximum the reflection coefficient

decrease up to 12eV is observed. At **e⊥c** polarization on ***R(E)*** spectrum two clear expressed maximums at 3.68eV and 4.58eV energies and minimum at 4.1eV energy are observed, ***R(E)*** decrease takes place up to energy 8.4eV and further its increase takes place.

The characteristic function of electron energy losses is defined by the following way:

$$-I_m\left(\frac{1}{\varepsilon}\right)=\frac{\varepsilon_i}{\varepsilon_i^2+\varepsilon_r^2},$$

The spectral characteristic of imaginary part of reverse value of complex dielectric constant $\left(I_m\left(-\varepsilon^{-1}\right)\right)$ is presented on fig.3b. From this it is seen that at **e||c** and **e⊥c** polarizations the change character I_m is similar one, i.e. I_m weakly increases with energy increase. With further energy increase up to 12eV the strong increase reverse to increase of complex dielectric constant takes place.

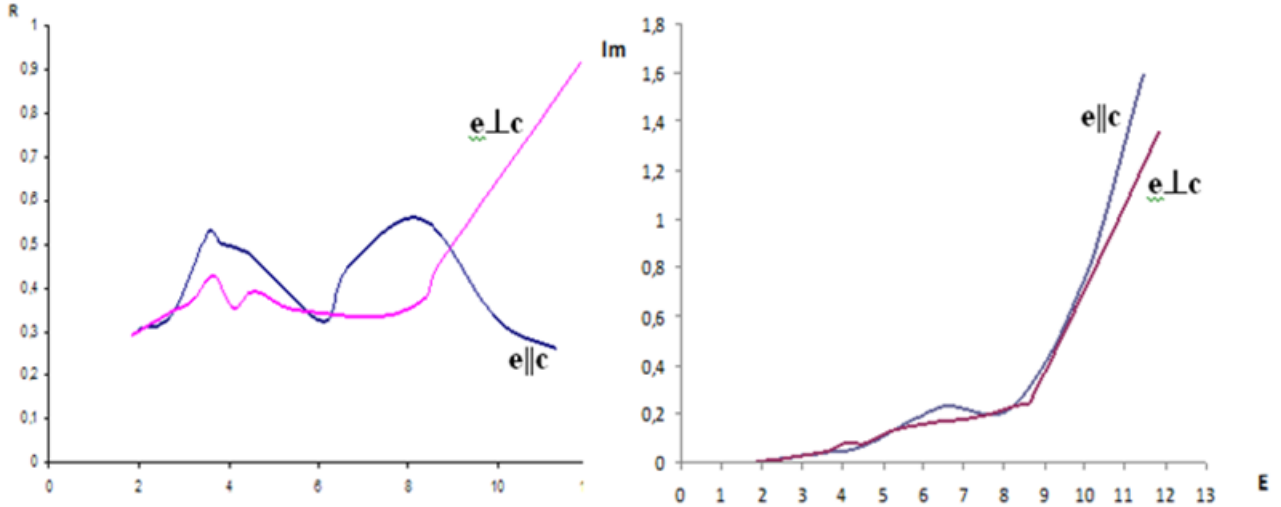

a) b)

Fig.3. The spectral dependence of reflection coefficient ***R(E)*** (a) and imaginary part of reverse value of complex dielectric constant I_m **(b)** of $InGaSe_2$ compound for **e||c** (**a**) and for **e⊥c** polarizations.

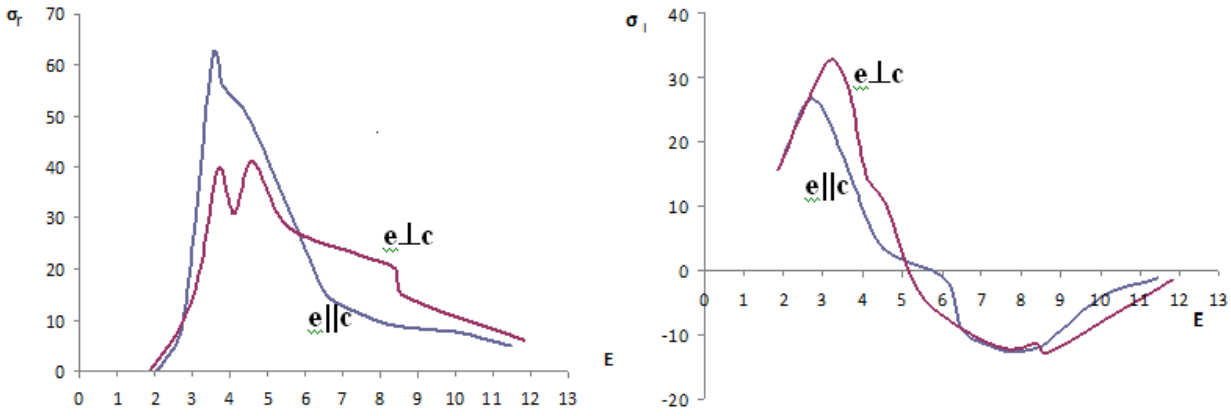

a) b)

Fig.4. The spectral dependence of real (a) and imaginary (b) of $\sigma_i(E)$optical electric conduction of $\sigma_i(E)$ $InGaSe_2$ compound for **e||c** and **e⊥c** polarizations.

The real and imaginary parts of optical electric conduction are defined with the help of following formula:

$$\sigma_r=\frac{\omega\varepsilon_i}{4\pi},\qquad \sigma_i=-\frac{\omega\varepsilon_r}{4\pi},$$

The results of their calculation are given on fig.4. As it is followed from fig.4a at **e||c** polarization on $\sigma_r(E)$ spectrum the only one clear expressed maximum at 3.54eV energies is observed.

With further energy increase firstly the strong energy decrease up to 6.63eV takes place and later the relative weak decrease $\sigma_r(E)$takes place.

At **e**⊥**c** polarization on $\sigma_r\ (E)$ curve at 3.68eV and 4.58eV energies two maximums are observed and between these maximums at energy 4.1eV is observed and in this case after second maximum decrease $\sigma_r(E)$ up to 12eV takes place.

The dependence $\sigma_i(E)$ at **e**||**c** and **e**⊥**c** polarizations is given on fig.4b. In this case the change character $\sigma_r(E)$ for both polarizations is similar one, i.e. at **e**||**c** polarization the clear maximum is observed at energy 2.7eV and at **e**⊥**c** polarization the maximum is observed at energy 3.2eV. In both cases $\sigma_r(E)$ decrease up to 8.2eV is observed and further the relative moderate increase of electric conduction is observed.

[1] *V. Capozzi, L. Pavesi and J. L. Staehli*, "Exi Ton-Carrier Scattering in Gallium Selenide," *Physical Review*, Vol. 47, No. 11, 1993, pp. 6340-6349.

[2] *M. Mobarak, H. Berger, G. F. Lorusso, V. Capozzi, G. Perna, M. M. Ibrahim and G. Margaritondo*, "The Growth and Properties of Single Crystals of GaInTe2, a Ternary Chalkogenide Semiconductor," *Journal of Physics D*: *Ap- plied Physics*, Vol. 31, No. 12, 1998, p. 1433-1437.

[3] *M. Mobarak, H. Berger, G. F. Lorusso, V. Capozzi, G. Perna, M. M. Ibrahim and G. Margaritondo*, "The Growth and Characterization of GaInSe2 Single Crystals," *Jour- nal of Physics D*: *Applied Physics*, Vol. 30, No. 18, 1997, pp. 2509-2516.

[4] *X. Gonze, J.-M. Beuken, R. Caracas, F. Detraux,*

[5] *M. Fuchs, G.-M. Rignanese, L. Sindic, M. Verstraete, G. Zerah, F. Jollet, M. Torrent, A. Roy, M. Mikami*, J.-Y. Ghosez and D. C. Raty, "First-Principles Computation of Material Properties: The ABINIT Software Project," *Computational* Materials Science, Vol. 25, No. 3, 2002, pp. 478-492.

[6] *E.M. Gojaev, Z.A. Jahangirli, P.F. Alieva, Kh.S. Khalilova, T.P. Musaev* The Growth of Single Crystals of $InGaSe_2$ Compounds, Their X-Ray-Phase Analysis, Electronic Structure and Optical Functions, Open Journal of Inorganic Non-Metallic Materials, 2013, p1-5.

[7] *Yu.I. Ukhanov*. Opticheskie svoystva poluprovodnikov. Moskva, Nauka, 1977, s. 335.

Received:07.11.2013

ISSN 1028-8546

2013, Vol. XIX, № 4
Section: En

CONTENTS